nature microbiology

Article

https://doi.org/10.1038/s41564-024-01647-4

Expanded phylogeny of extremely halophilic archaea shows multiple independent adaptations to hypersaline environments

Received: 30 June 2023

Accepted: 20 February 2024

Published online: 22 March 2024

Check for updates

Brittany A. Baker[1], Ana Gutiérrez-Preciado[1], Álvaro Rodríguez del Río[2], Charley G. P. McCarthy[3,4], Purificación López-García[1], Jaime Huerta-Cepas[2], Edward Susko[3,5], Andrew J. Roger[3,4], Laura Eme[1] & David Moreira[1]

Extremely halophilic archaea (Haloarchaea, Nanohaloarchaeota, Methanonatronarchaeia and Halarchaeoplasmatales) thrive in saturating salt concentrations where they must maintain osmotic equilibrium with their environment. The evolutionary history of adaptations enabling salt tolerance remains poorly understood, in particular because the phylogeny of several lineages is conflicting. Here we present a resolved phylogeny of extremely halophilic archaea obtained using improved taxon sampling and state-of-the-art phylogenetic approaches designed to cope with the strong compositional biases of their proteomes. We describe two uncultured lineages, Afararchaeaceae and Asbonarchaeaceae, which break the long branches at the base of Haloarchaea and Nanohaloarchaeota, respectively. We obtained 13 metagenome-assembled genomes (MAGs) of these archaea from metagenomes of hypersaline aquatic systems of the Danakil Depression (Ethiopia). Our phylogenomic analyses including these taxa show that at least four independent adaptations to extreme halophily occurred during archaeal evolution. Gene-tree/species-tree reconciliation suggests that gene duplication and horizontal gene transfer played an important role in this process, for example, by spreading key genes (such as those encoding potassium transporters) across extremely halophilic lineages.

For decades, all known extremely halophilic archaea (growing at salt concentrations >30% w/v) belonged to the Halobacteria[1,2] (henceforth Haloarchaea). Recently, metagenomics uncovered additional groups, whose phylogenetic positions have been unclear (Extended Data Fig. 1): (1) Nanohaloarchaeota[3–5], tiny symbiotic archaea initially thought to be closely related to the Haloarchaea but placed later in the DPANN super-group[6], suggesting an independent adaptation to extreme salinity; (2) Methanonatronarchaeia[7], a class of extremely halophilic methanogens, initially proposed to be an 'evolutionary intermediate' between non-halophilic Class II methanogens and Haloarchaea, but

[1]Ecologie Systématique Evolution, CNRS, Université Paris-Saclay, AgroParisTech, Gif-sur-Yvette, France. [2]Centro de Biotecnología y Genómica de Plantas, Universidad Politécnica de Madrid (UPM) - Instituto Nacional de Investigación y Tecnología Agraria y Alimentaria (INIA-CSIC), Madrid, Spain. [3]Institute for Comparative Genomics, Dalhousie University, Halifax, Nova Scotia, Canada. [4]Department of Biochemistry and Molecular Biology, Dalhousie University, Halifax, Nova Scotia, Canada. [5]Department of Mathematics and Statistics, Dalhousie University, Halifax, Nova Scotia, Canada. e-mail: laura.eme@universite-paris-saclay.fr; david.moreira@universite-paris-saclay.fr

placed at the base of Methanotecta in more recent studies[8–11]; and (3) Halarchaeoplasmatales[12], an order robustly placed within Thermoplasmatota. These extremely halophilic archaea have evolved unique strategies to cope with osmotic stress: they pump high levels of potassium into their cells[13] and maintain acidic proteomes, rich in aspartic and glutamic acids and depleted in basic and large hydrophobic amino acids[14–17]. These amino acid usage biases and the higher evolutionary rate at the base of halophilic archaea can lead to long-branch attraction (LBA) and other phylogenetic reconstruction artefacts, resulting in conflicting evolutionary relationships[9,18,19]. Thus, how many times these adaptations evolved remains enigmatic. Here we introduce two previously undescribed families of extreme halophiles, Afararchaeaceae and Asbonarchaeaceae. With sophisticated methods and broader taxonomic sampling, we establish a comprehensive phylogeny of halophilic archaea. Our updated scenario highlights at least four independent adaptations to hypersaline environments and emphasizes the adaptive role of horizontal gene transfer (HGT) between different halophilic groups.

Results

Two previously undescribed groups of halophilic archaea

The Danakil Depression (Afar region, Ethiopia) contains hypersaline lakes hosting extremely halophilic archaea[20,21]. Among the metagenome-assembled genomes (MAGs) reconstructed from these lakes, we identified 13 belonging to two lineages of extreme halophiles phylogenetically distant from already known groups, plus one additional MAG placed deep in the Haloarchaea (Fig. 1a,c and Supplementary Data 1).

The first group, a family-level lineage named Afararchaeaceae (after Ethiopia's Afar region), was represented by four moderately GC-rich (53–60%) MAGs with average nucleotide identity (ANI) values between 72 and 74% between them (Supplementary Data 2 and Fig. 1a,b). Afararchaeaceae branched with maximal support as a sister lineage to the group UBA12382 (or 'hikarchaea'[10])+Haloarchaea (Fig. 1a and Supplementary Fig. 2). Initially described as intermediates between non-halophilic methanogens and Haloarchaea[10], this result suggests that hikarchaea adapted secondarily to low salinity from an extremely halophilic ancestor.

The most complete afararchaeal MAG (DAL-WCL_na_97C3R), formally named *Afararchaeum irisae* gen. nov., sp. nov. (see description below), had a size of ~1.9 Mbp (Supplementary Data 1). KEGG annotation[22] indicates that Afararchaeaceae are probably heterotrophic aerobes that utilize branched-chain amino acids as a carbon source, similar to many known Haloarchaea[23] (Fig. 1b and Supplementary Data 3). They are likely mobile, possessing all genes for the archaeal flagellum (archaellum)[24] and a chemotaxis operon. In addition, afararchaeal MAGs encode a single type-II sensory rhodopsin for phototaxis[25] but lack bacteriorhodopsin genes, suggesting that these archaea do not use light as an additional energy source like many Haloarchaea[26]. As expected, Afararchaeaceae probably employ a salt-in osmoregulation involving multiple K^+ transporters (eight Trk-like and two Kef-like), mechanosensitive ion channels (MscS and MscL) and Na^+/Ca^{2+} exchangers (Supplementary Data 2). Consequently, they also exhibit a highly acidic proteome (Fig. 2a,b).

The second group comprises nine MAGs (46–64% GC content) with ANI values between 74 and 79% between them (Supplementary Data 2 and Fig. 1c,d). They branched as a sister group to the DPANN family Nanosalinaceae (Fig. 1c and Supplementary Fig. 3) and are related to MAGs that were previously classified as 'Nanoanaerosalinaceae' and 'Nanohalalkaliarchaeaceae'[5] (Supplementary Fig. 4). However, these two families have been merged within the family 'JALIDP01' in the Genome Taxonomy Database (GTDB)[27]. Our MAGs provide substantial coverage of this family, with three related to the former 'Nanoanaerosalinaceae' and six to the single MAG representing the 'Nanohalalkaliarchaeaceae'[5] (Supplementary Fig. 4). Given this taxonomic uncertainty and their presence in both anoxic[5] and oxic (this work) environments, we propose formally naming this family Asbonarchaeaceae, derived from '*asbo*', meaning salt in the Afar language, acknowledging their consistent presence in hypersaline systems.

DPANN genomes, like those in the Asbonarchaeaceae, typically lack certain genes, leading to an underestimated genome completeness, typically up to ~85%[19,28]. We thus probably obtained a nearly complete asbonarchaeal MAG (DAL-WCL_45_84C1R, 84% complete) representing the type species for this family, *Asbonarchaeum danakilense* gen. nov., sp. nov. (see description below), with a genome size of 1.2 Mbp, similar to other DPANNs[19] (Supplementary Data 1). Asbonarchaeaceae lack crucial biosynthetic pathways (lipid, nucleotide and amino acid biosynthesis), suggesting that they live symbiotically, relying on a host like other DPANN groups[29–31] (Fig. 1d and Supplementary Data 4). They lack a canonical electron transport chain but possess all essential subunits of a V/A-type ATP synthase (Fig. 1d)[29]. We again predict that Asbonarchaeaceae employ salt-in osmoregulation with multiple K^+ transporters (Supplementary Data 4) and a highly acidic proteome (Fig. 2a,b). Despite their phylogenetic relationship with the Nanosalinaceae, they display a distinct amino acid composition (Fig. 2a), confirming their status as an independent family within the Nanohaloarchaeota.

Undescribed gene families in Afararchaeaceae and Asbonarchaeaceae

We identified previously undescribed gene families using a two-step approach. First, we searched for genes in Afararchaeaceae and Asbonarchaeaceae genomes with no detectable homologues in sequence databases of cultured organisms (RefSeq[32], Pfam[33] and EggNOG[34]), revealing a large number of potentially unique genes (10–30% of their total genes; Extended Data Fig. 2a). Second, we compared these genes against a vast collection of 169,529 prokaryotic genomes[35], confirming that only 14% (Asbonarchaeaceae) and 17.1% (Afararchaeaceae) have related genes in other uncultured species, highlighting many unknown lineage-specific genes (Supplementary Data 4 and 5). Notably, these genes encode proteins with an acidic pH isoelectric point, aligning with adaptation to hypersaline environments[36] (Extended Data Fig. 2b). A considerable percentage of these proteins contain transmembrane domains or signal peptides, probably targeting them to the membrane or extracellular space, directly interacting with the external high salt concentrations. We analysed their genomic context to predict their functions. Approximately 5% (Afararchaeaceae) and 18% (Asbonarchaeaceae) of them have conserved synteny and co-localize with genes with known functions, indicating roles related to those of their neighbouring genes (Supplementary Data 5 and 6). For example, we found a protein in Afararchaeaceae next to a mechanosensitive ion channel (Fig. 1e), suggesting a potential role in osmotic regulation[37].

A conserved core of archaeal phylogenetic markers

Previous attempts to determine the phylogenetic placement of extreme halophiles mainly relied on limited datasets such as single genes[3,9] or concatenated ribosomal proteins[7,10]. However, these small datasets contain few sites and provide limited phylogenetic information[18,38]. Moreover, ribosomal proteins may have compositional biases that differ from the rest of the proteome due to their complex protein–protein and protein–RNA interactions[18,39]. To address these issues and accurately determine the positions of extreme halophilic archaea, we conducted comprehensive phylogenomic analyses using a dataset of 136 non-ribosomal marker proteins (NM dataset; 39,385 positions) highly conserved among archaea[18]. These proteins serve various functions (Supplementary Data 7), reducing potential biases linked to co-evolution patterns. On the basis of individual phylogenetic trees, we manually curated our NM marker set to exclude possible HGT or hidden paralogy (see Methods). In addition, we curated a set of 48 ribosomal

https://doi.org/10.1038/s41564-024-01647-4

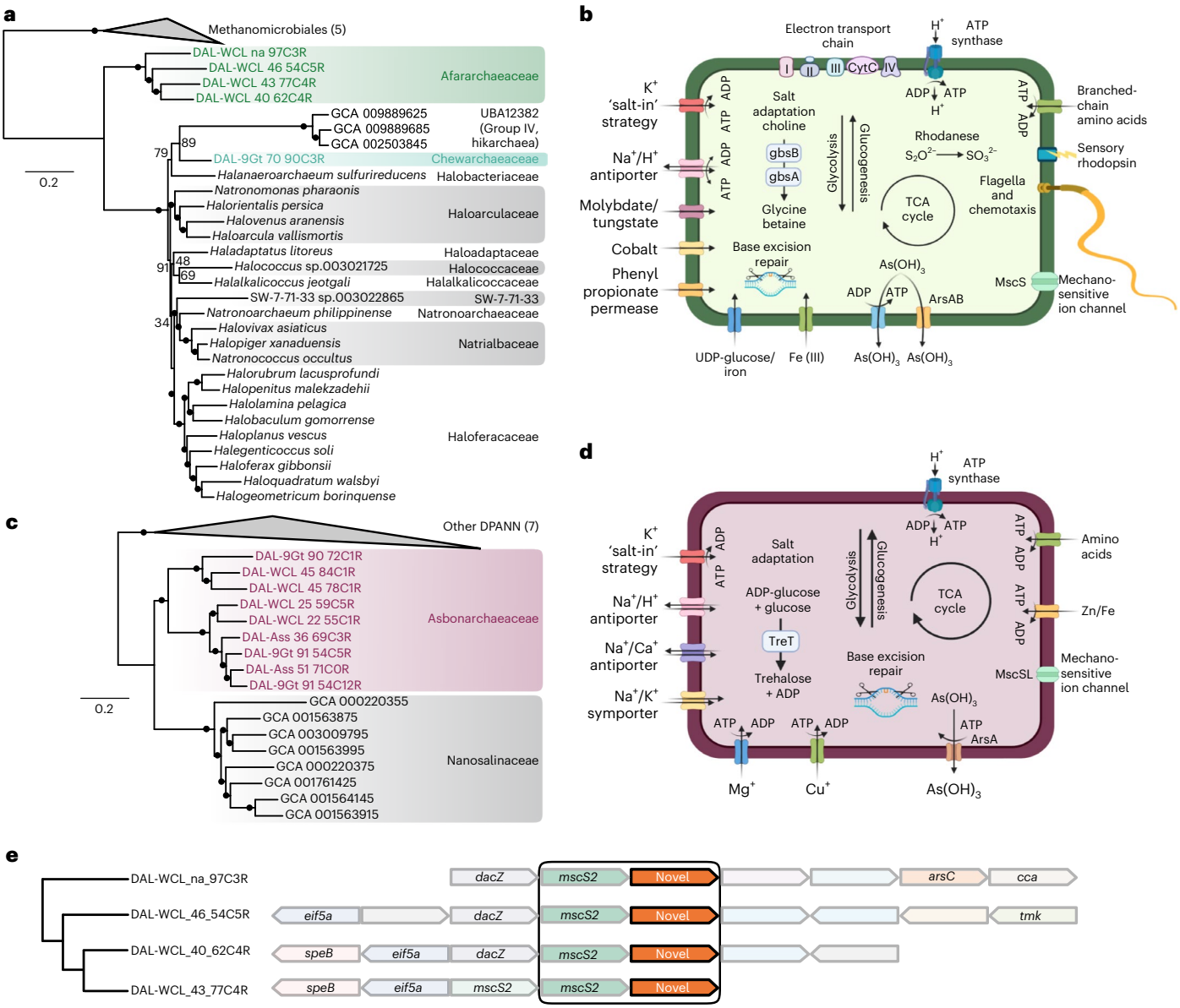

Fig. 1 | Phylogenetic position and metabolic potential of the families Afararchaeaceae and Asbonarchaeaceae. a, Maximum likelihood phylogenetic tree of 35 Euryarchaeota, including four Afararchaeaceae MAGs (highlighted in green), based on the concatenation of 122 single-copy proteins obtained from the GTDB. The tree was inferred via IQ-TREE with the LG + C60 + F + Γ4 model of sequence evolution. The statistical support for branches, with filled circles representing values equal to or larger than 99% support, corresponds to 1,000 ultrafast bootstrap replicates. The scale bar indicates the expected average number of substitutions per site. All taxonomic ranks shown are based on the GTDB r207 family-level classification. See Supplementary Fig. 2 for the uncollapsed tree. **b**, Non-exhaustive metabolic scheme based on the predicted gene content of the most complete afararchaeal MAG (DAL-WCL_na_97C3R). A detailed table of the predicted gene content can be found in Supplementary Table 3. **c**, Maximum likelihood phylogenetic tree of 24 DPANN archaea, including nine Asbonarchaeaceae MAGs (highlighted in wine), based on the concatenation of 99 single-copy proteins obtained from the GTDB. The tree was inferred by IQ-TREE with the LG + C60 + F + Γ4 model of sequence evolution. The statistical support for branches corresponds to 1,000 ultrafast bootstrap replicates. The scale bar indicates the expected average number of substitutions per site. All taxonomic ranks are based on the GTDB r207 family-level classification. See Supplementary Fig. 3 for the uncollapsed tree. **d**, Non-exhaustive metabolic scheme based on the predicted gene content of the most complete asbonarcharchaeal MAG (DAL-WCL_45_84C1R). A detailed table of the predicted gene content can be found in Supplementary Table 4. **e**, Gene maps showing a previously undescribed gene family (orange) linked to a conserved mechanosensitive ion channel (*mscS2*) in the afararchaeal MAGs. *speB*, agmatinase; *eif5a*, eukaryotic initiation factor 5A; *dacZ*, di-adenylate cyclase; *arsC*, arsenate reductase; *cca*, tRNA nucleotidyltransferase; *tmk*, thymidylate kinase.

proteins (RP dataset, 6,792 positions) to compare their phylogenetic signal with that of the NM dataset.

Testing the influence of taxon sampling

Extreme halophilic archaea often display long branches, potentially yielding artefactual placements due to LBA[40,41]. To address this, we employed different datasets and approaches. In addition to the full dataset (Fig. 3a, and Extended Data Figs. 3 and 4), we used smaller taxon samplings, focusing on specific archaeal groups such as Euryarchaeota only (including Afararchaeaceae) and Euryarchaeota+Nanohaloarchaeota (Supplementary Figs. 5–8 and Data 8). The corresponding phylogenies revealed congruent placements for all extreme halophiles except Methanonatronarchaeia. NM-based maximum likelihood (ML) trees grouped them with

https://doi.org/10.1038/s41564-024-01647-4

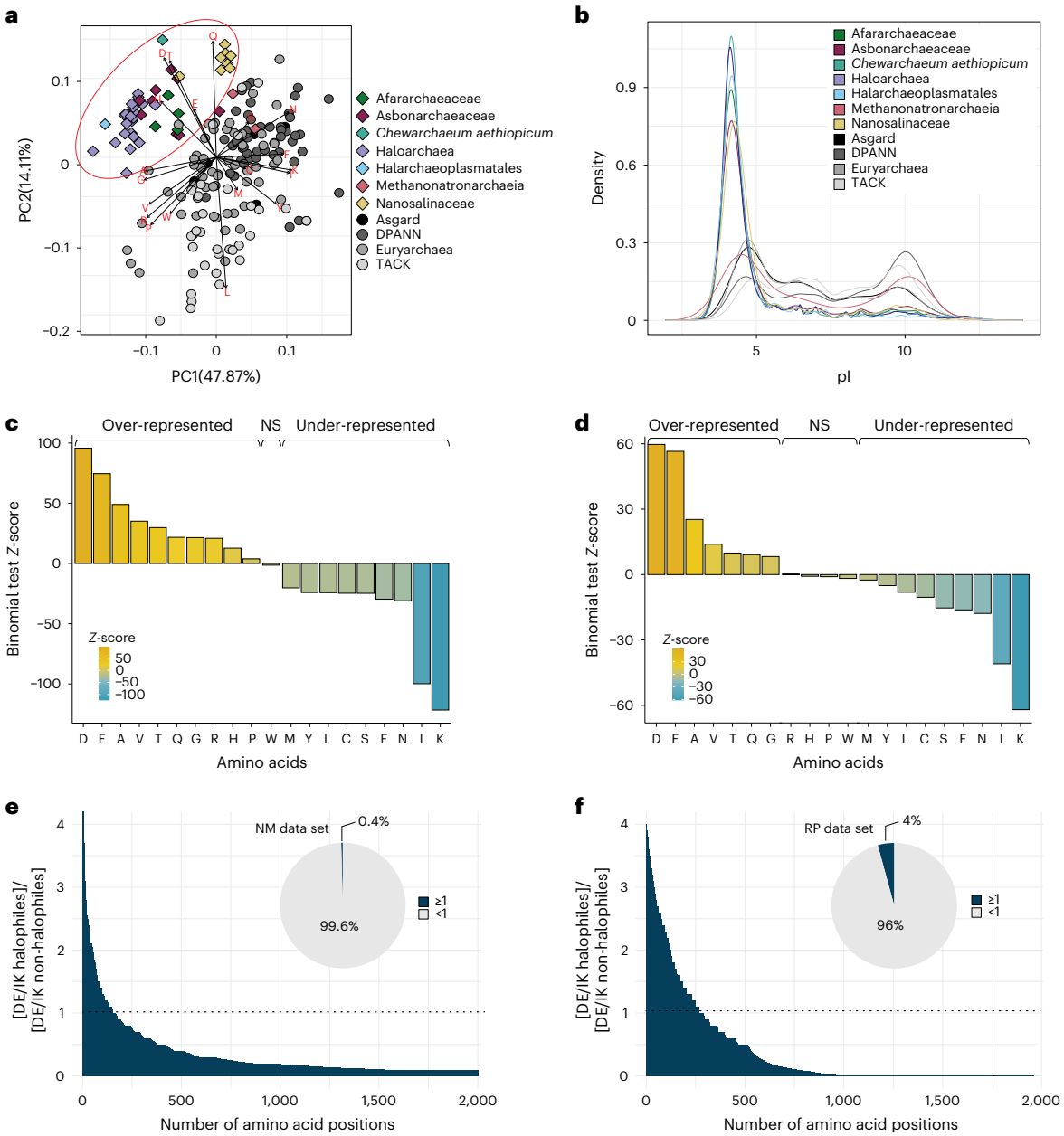

Fig. 2 | Protein amino acid compositional biases in extremely halophilic archaeal lineages. a, PCA plot of 192 archaeal proteomes based on amino acid frequencies. The red ellipse indicates the clustering of extreme halophiles (coloured diamonds), including the families Afararchaeaceae (green colour) and Asbonarchaeaceae (wine colour). **b**, Isoelectric point (pI) distribution of 192 archaeal proteomes. Non-halophilic archaea (grey lines) display a bimodal distribution of pI values, while extreme halophiles (coloured lines) exhibit a single spike at pI ~4, indicating a highly acidic proteome. **c**,**d**, Binomial tests for the (**c**) NM and (**d**) RP datasets, they compare the proportions of all 20 amino acids between extreme halophiles and non-halophiles. *Z*-scores were calculated relative to extreme halophiles, with |Z| > 1.96 indicating significant enrichment of a given amino acid in extreme halophile sequences ('Over-represented'), |Z| < −1.96 indicating significant depletion of a given amino acid in extreme halophile sequences ('Under-represented'), and some amino acids showing no significant bias ('NS'). **e**,**f**, D + E/I + K site-by-site bias (defined as the ratio [D + E/I + K for extreme halophiles]/[D + E/I + K for non-halophiles]) for the 2,000 most biased sites of the (**e**) NM dataset (39,385 amino acid positions) and (**f**) RP dataset (6,792 amino acid positions). Inset pie charts depict the proportion of amino acids with a ratio greater than or equal to 1 (dark blue) versus less than 1 (grey).

Methanotecta (that is, Haloarchaea, 'hikarchaea', Class II methanogens, Methanopagales, ANME-1, Synthrophoarchaeales and Archaeoglobales) or with the Afararchaeaceae+'hikarchaea'+Haloarchaea (AHH) clade, while RP-based ML trees placed them as sisters to the AHH clade. The two topologies were significantly different based on an approximately unbiased (AU) test[42] since the NM topology was rejected on the basis of the RP alignment (*P* value = 0.0000431) and the RP topology was rejected on the basis of the NM alignment (*P* value = 0.0000165). Bayesian analyses, with four Markov chain Monte Carlo (MCMC) chains each and applying the complex CAT + GTR model, showed similar conflicting placements (Supplementary Figs. 9–12), highlighting how different taxon samplings, models and phylogenetic frameworks can showcase conflicting signals in phylogenetic analyses of Methanonatronarchaeia. These results underscore the challenges in placing extreme halophiles accurately, most probably because of their unique compositional biases linked to their 'salt-in' osmoregulation strategy[14–17], which are not properly accounted for by standard substitution models[43].

https://doi.org/10.1038/s41564-024-01647-4

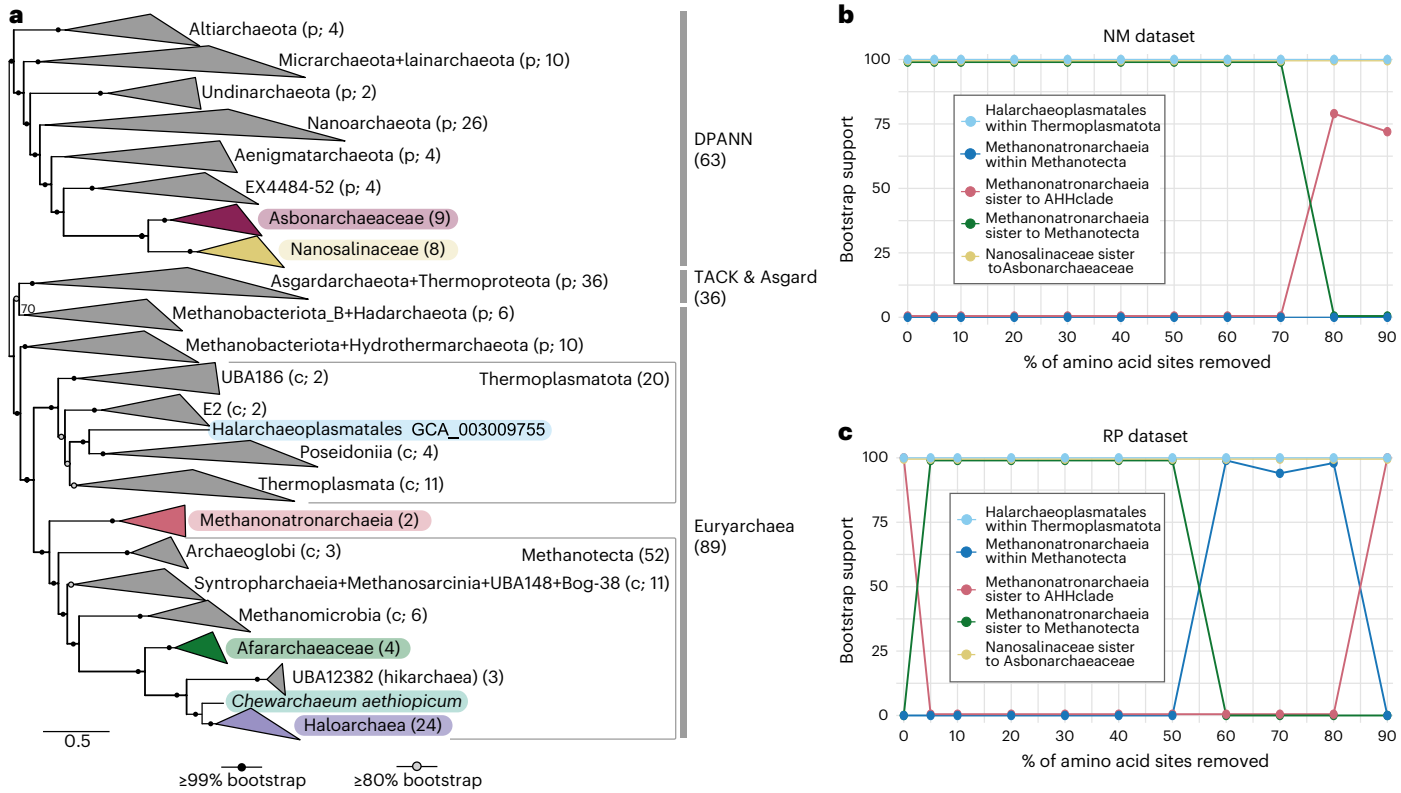

Fig. 3 | Maximum likelihood phylogeny of archaea, including the Afararchaeaceae and Asbonarchaeaceae. a, Phylogenetic tree based on the concatenation of 136 conserved markers (NM dataset) across 192 taxa (39,385 sites) via IQ-TREE under the LG + C60 + F + Γ4 model. Statistical support indicated on the branches corresponds to 1,000 ultrafast bootstrap replicates. The scale bar indicates the number of substitutions per site. Colours indicate the currently known groups of extremely halophilic archaea. The taxonomic level (p, phyla; c, class) and the size of collapsed clades are indicated in parentheses; see Extended Data Fig. 3 for the uncollapsed tree. **b**,**c**, Impact of the progressive removal (in steps of 10%) of the most compositionally biased sites from the (**b**) 192-NM (39,385 amino acid positions) and (**c**) 192-RP (6,792 amino acid positions) datasets. Lines show the statistical support values for the position of each of the halophilic clades of interest. These support values were estimated using the ultrafast bootstrap approximation from the ML tree reconstruction (LG + C60 + F + Γ4 model) for each site-removal step.

Addressing the effect of compositional biases

Model misspecification induced by compositional bias is a known source of phylogenetic error. To reduce potential LBA artefacts affecting extreme halophiles, previous studies either recoded data into four character states[10,44] or removed the fastest-evolving sites[8,10,44]. However, the latter method resulted in the loss of up to 50% of alignment sites, which is problematic for small datasets such as the RP-based ones[11]. Therefore, we explored two alternative approaches to address halophile-specific compositional biases while preserving substantial phylogenetic information.

First, we identified amino acids significantly over or under-represented in extreme halophiles compared with non-halophiles in the 192-taxa NM and RP datasets. D + E and I + K were the most over and under-represented amino acids, respectively (Fig. 2c,d). We then applied a variation of the GFmix model[43] to cope with these specific compositional biases. GFmix is a site-heterogeneous mixture model that adjusts amino acid frequencies for each class of the mixture model in a branch-specific manner to accommodate shifts in amino acid composition over the branch. Amino acids were categorized into three groups: those that increased, decreased or remained unchanged in frequency on the branch. We used the LG + C60 + F + Γ4 model with GFmix (GFmix-DE/IK model), where [D + E]/[I + K] compositional ratio varied over branches. Despite improvements in likelihood values under this model, the RP and NM datasets remained incongruent regarding the position of Methanonatronarchaeia (Supplementary Fig. 13). We also explored a GFmix variant with larger groups of significantly over and under-represented amino acids (Fig. 2c,d). Although it further improved the likelihood, the relative preferences of topologies for each dataset remained unchanged (Supplementary Fig. 13).

Our second approach involved the gradual removal of highly compositionally biased alignment sites. We calculated the D + E/I + K ratio for halophilic versus non-halophilic lineages, ranked the sites accordingly and then progressively removed the most biased sites. For the 192-taxa NM dataset, the position of Methanonatronarchaeia remained unchanged until 80% of sites were removed, after which they branched as the sister group of the AHH clade with weak support (Fig. 3b). By contrast, for the 192-taxa RP dataset, Methanonatronarchaeia shifted to a fully supported sister position to Methanotecta with only 5% of the most biased sites removed (Fig. 3c). This is congruent with the observation that the RP dataset has a higher proportion of sites with biased D + E/I + K ratios compared to the NM dataset (4% versus 0.4% of positions with a ratio ≥1, respectively) (Fig. 2e,f and Extended Data Fig. 5).

We examined the ribosomal proteins with the most biased sites (for example, L1, L12e, S6 and S15) and found that they were located on the outer surface of the ribosomal complex, in close interaction with the K^+-rich cytoplasm (Supplementary Fig. 14 and Video 1). To confirm the impact of the D + E/I + K bias on the RP-based phylogeny, we inferred an ML tree using a concatenation of the 18 most biased ribosomal proteins, which resulted in all extremely halophilic groups clustering with 100% support (Supplementary Fig. 15). We also reconstructed Bayesian phylogenies with 20% of the most biased alignment sites removed for both the 104-NM and 104-RP datasets. Contrary to trees constructed with the untreated datasets (see above), all MCMC chains for both datasets supported the deeper-branching position

https://doi.org/10.1038/s41564-024-01647-4

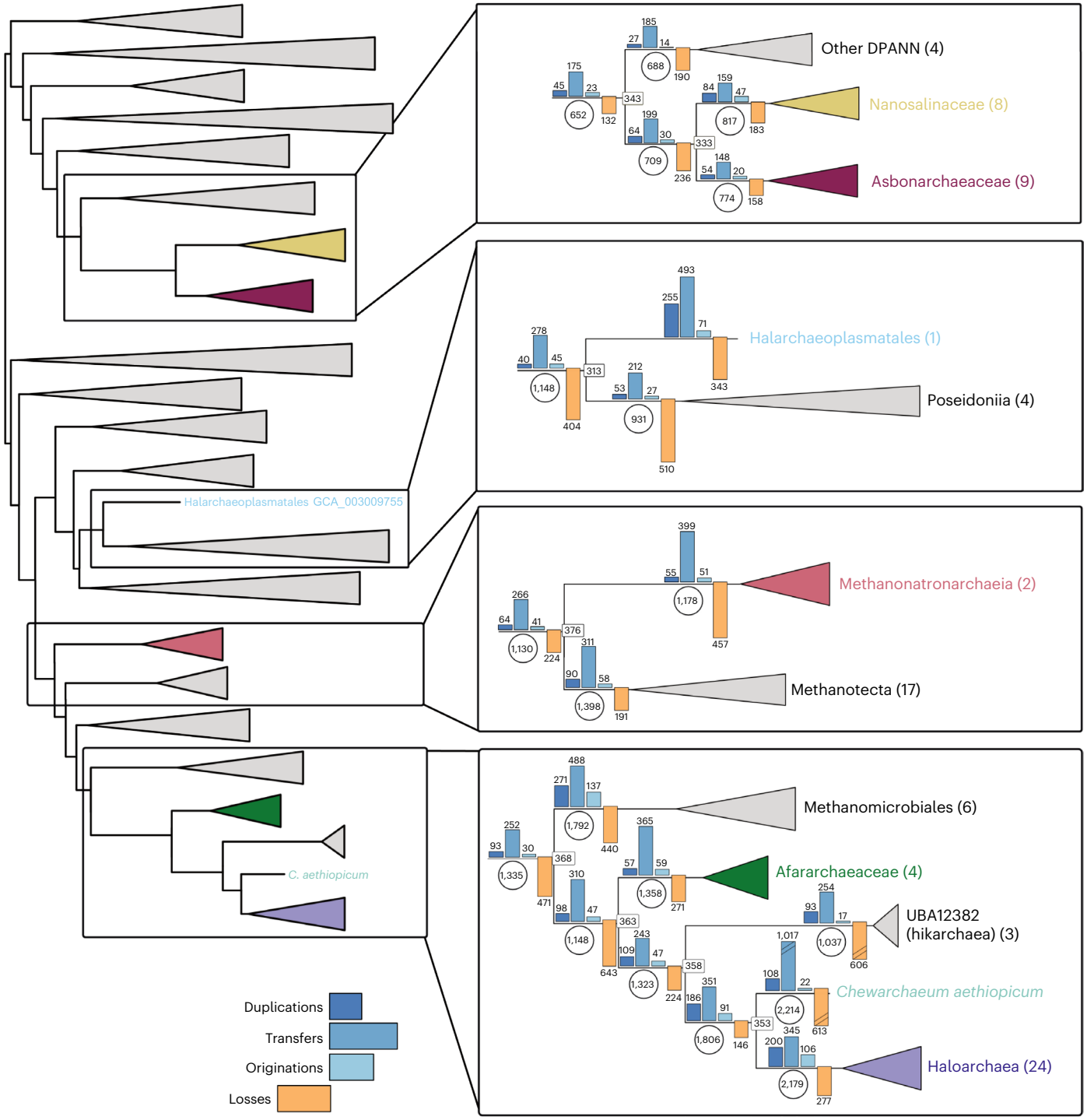

Fig. 4 | Schematic representation of the tree reconciliation analysis based on the NM species tree. The full archaeal tree is shown on the left; boxes on the right highlight the details for the four main groups of halophilic archaea: Nanosalinaceae+Asbonarchaeaceae, Halarchaeoplasmatales, Methanonatronarchaeia and Afararchaeaceae+Haloarchaea. The bar plots on the branches represent the number of gene duplications, transfers, originations and losses, and the circles indicate the number of predicted ancestral gene copy numbers. The number of taxa in each collapsed clade is indicated by the number in parentheses next to the clade name. The complete version of this tree with the events for all archaeal nodes can be found in Supplementary Fig. 18.

of Methanonatronarchaeia sister to Methanotecta (Supplementary Figs. 16 and 17).

A recent study suggested that, given their slow evolutionary rate and their belonging to a single complex, ATP synthase subunits A and B are less susceptible to phylogenetic artefacts[9]. A phylogeny based on the concatenation of both subunits supported the Nanohaloarchaeota sister to Haloarchaea[9,45]. However, when we removed 15% of the highest D + E/I + K ratio sites from this dataset, Nanohaloarchaeota branched deeper (Extended Data Fig. 6), indicating that a few highly biased sites artificially drove their position close to Haloarchaea.

In conclusion, our phylogenomic analyses, especially those mitigating the strong convergent compositional bias shared by the halophilic lineages, robustly support at least four independent adaptations to extreme halophily in archaea: in the AHH clade, Methanonatronarchaeia, Halarchaeoplasmatales and Nanosalinaceae+Asbonarchaeaceae.

Gene content evolution in archaeal extreme halophiles

We used the amalgamated likelihood estimation (ALE) method to examine gene content evolution in the 192-taxa dataset. By reconciling individual gene trees with the species tree (Fig. 3a), we estimated gene duplications, transfers, originations, losses and copy numbers at all ancestral nodes. This approach included Methanonatronarchaeia, previously excluded from similar analyses due to their unresolved phylogenetic position[10]. Gene transfer and loss appear to be the primary drivers of gene content evolution in archaea, including halophilic groups (Fig. 4, Extended Data Fig. 7 and Supplementary Fig. 18). Haloarchaea, with some of the largest genome sizes among archaea[46], also experienced significant gene originations and duplications during their early evolution. This expansion involved genes encoding key inorganic ion transporters (Trk and Kef-type K^+ transporters, Mg^{2+} transporters, SSF Na^+/solute symporters, NhaP-type K^+/H^+ antiporters, Ca^+/Na^+ and Na^+/H^+ antiporters) crucial for osmotic regulation (Supplementary Figs. 19–26 and Extended Data Fig. 8a), and molecular chaperones such as GrpE (Supplementary Fig. 27), which prevents protein aggregation during response to hyperosmotic stress[47]. Amino acid transporters, vital for species of these groups thriving on amino acids[23], also exhibited duplications (Extended Data Fig. 7). Presence probabilities estimated by ALE at key halophilic ancestors are reported for each of these proteins in Supplementary Data 9.

Halarchaeoplasmatales also had numerous gene duplications, spanning metabolism and informational processes such as transcription, DNA replication and repair (Extended Data Fig. 7). In Nanosalinaceae and Asbonarchaeaceae, gene transfer was dominant but less pronounced due to constraints in these small-sized archaea to maintain compact genomes[48]. By contrast, the 'hikarchaea' displayed extensive gene loss, which supports the hypothesis that these marine archaea evolved from extremely halophilic ancestors (the Hik-Haloarchaea ancestor with 1,323 inferred protein-coding genes, Fig. 4) and adapted to nutrient-poor deep-sea environments through gene loss, typical of many streamlined marine prokaryotes[49,50]. Nevertheless, this adaptation also included duplications of specific genes linked to energy production, conversion, and carbohydrate and amino acid transport and metabolism (Extended Data Fig. 7). Notably, we observed multiple copies of aerobic-type carbon monoxide dehydrogenase, found in other microorganisms adapted to the same nutrient-poor environments[51] (Supplementary Fig. 28).

Massive HGT from bacteria has probably played an important role in the evolution of Haloarchaea, although its extent and timing are still debated[52–55]. Several transfers happened before the split between Afararchaeaceae and Haloarchaea, facilitating the adaptation of their common ancestor to extreme halophily. For instance, the choline dehydrogenase BetA, involved in the synthesis of the osmoprotectant glycine-betaine[56], was acquired through HGT (Extended Data Fig. 8b). Notably, this gene is absent in hickarchaea, reinforcing the idea of gene loss during their secondary adaptation to low-salt environments. Another example is a BCCT family transporter involved in osmoprotectant uptake, such as glycine betaine[56], which Methanonatronarchaeia acquired from bacteria (Supplementary Fig. 29).

HGT between Haloarchaea and other halophilic archaea has also played a role in their convergent adaptations to extreme salinity. Examples include the chaperone GrpE and various multicopy transporters such as K^+ (Trk- and Kef-type) and Mg^{2+} transporters, and K^+/H^+, Ca^{2+}/Na^+ and Na^+/H^+ antiporters. In addition, other inorganic molecule transporters have been transferred among halophilic archaeal groups, such as SNF-family Na^+-dependent transporters, ZupT and FieF-type metal transporters, sulfur transporters, Na^+/H^+ antiporters and Na^+/phosphate symporters (Supplementary Figs. 30–36).

HGT of organic molecule transporters is also observed, such as a transporter of Krebs cycle intermediates shared by Haloarchaea and Asbonarchaeaceae (Supplementary Fig. 37). We also identified genes of bacterial origin encoding various transporters subsequently transferred between different halophilic archaeal groups. These include genes encoding an AmiS/UreI urea transporter transferred between Haloarchaea and Nanohaloarchaea, and a TauE/SafE sulfite exporter transferred between Haloarchaea and Methanonatronarchaeia (Supplementary Figs. 38 and 39), consistent with previous reports of interdomain HGT followed by intradomain HGT[57].

Discussion

Our study yields a robust archaeal phylogeny, including two previously unknown halophilic lineages, Asbonarchaeaceae (closely related to Nanosalinaceae within the DPANN) and Afararchaeaceae (closely related to the Haloarchaea + 'hikarchaea' group). The position of Afararchaeaceae challenges the previous notion of 'hikarchaea' being intermediates between methanogens and haloarchaea[10], as they instead adapted secondarily to low salinity from extremely halophilic ancestors. Our phylogenomic analyses also position Methanonatronarchaeia as sister to Methanotecta, not as intermediates between Class II methanogens and haloarchaea[7]. Thus, we identify four independent adaptations to extreme halophily in archaea: in Haloarchaea+Afararchaeaceae, Methanonatronarchaeia, Halarchaeoplasmatales and Nanosalinaceae+Asbonarchaeaceae. All these adaptations involve a salt-in strategy with convergent independent extensive proteome acidifications. In addition, HGT played a crucial role in spreading key genes, such as those encoding ion transporters, among these halophilic lineages. This prompts the question of whether the initial adaptations to extreme halophily occurred as a singular event in one group, spreading through HGT to the other groups, and which lineage of extreme halophiles emerged first. Answering these intriguing questions will require further investigation of adaptive genes and their distribution in known and still undescribed halophilic archaea.

Taxonomic descriptions

Taxon names have been described under the SeqCode[58] as follows:

***Afararchaeum* gen. nov. Etymology.** *archaeum* (N.L. neut. n.): an archaeon; *Afararchaeum* (N.L. neut. n.): an archaeon from the Afar region. Type species. *Afararchaeum irisae*.

***Afararchaeum irisae* sp. nov. Etymology.** *irisae* (N.L. gen. n): named after the Iris Foundation (France), which supports the study and preservation of endangered ecosystems including those in the Afar region. The designated type MAG is DAL-WCL_na_97C3R.

Diagnosis. This archaeon lives in oxic hypersaline waters. It encodes genes for aerobic respiration and probably uses amino acids for organoheterotrophic growth. Its genome is ~1.9 Mbp (GC content: 55%). It is known from environmental sequencing only.

Afararchaeaceae fam. nov. Etymology. *Afararchaeum* (N.L. neut. n.): a genus name; -aceae, ending to denote a family; Afararchaeaceae (N.L. fem. pl. n.): the *Afararchaeum* family.

***Asbonarchaeum* gen. nov. Etymology.** *Asbo* (Afar language): salt; *archaeum* (N.L. neut. n.): an archaeon; *Asbonarchaeum* (N.L. neut. n.): a salt archaeon. Type species. *Asbonarchaeum danakilense*.

***Asbonarchaeum danakilense* sp. nov. Etymology.** *danakilense* (N.L. neut. adj.): pertaining to the Danakil Depression. The designated type MAG is DAL-WCL_45_84C1R.

Diagnosis. This halophilic archaeon lives in oxic hypersaline waters of the Danakil Depression. It has a ~1.2 Mb streamlined genome (GC content: 61%). It lacks most biosynthetic pathways, most probably growing as a symbiont of an unknown host. It is known from environmental sequencing only.

Asbonarchaeaceae fam. nov. Etymology. *Asbonarchaeum* (N.L. neut. n.): a genus name; -aceae, ending to denote a family; Asbonarchaeaceae (N.L. fem. pl. n.): the *Asbonarchaeum* family.

***Chewarchaeum* gen. nov. Etymology.** *Chew* (Amharic language): salt; *archaeum* (N.L. neut. n.): an archaeon; *Chewarchaeum* (N.L. neut. n.): a salt archaeon. Type species: *Chewarchaeum aethiopicum*.

***Chewarchaeum aethiopicum* sp. nov. Etymology.** *aethiopicum* (L. neut. adj): Ethiopian. The designated type MAG is DAL-9Gt_70_90C3R.

Diagnosis. This halophilic archaeon lives in oxic hypersaline waters of the Danakil Depression. It encodes genes for aerobic respiration and probably uses amino acids for organoheterotrophic growth. Its genome is ~2.9 Mb (GC content: 61%). It is known from environmental sequencing only.

***Chewarchaeaceae* fam. nov. Etymology.** *Chewarchaeum* (N.L. neut. n.): a genus name; -aceae, ending to denote a family; Chewarchaeaceae (N.L. fem. pl. n.): the *Chewarchaeum* family.

Methods

Selection of metagenome-assembled genomes

We searched for MAGs related to known groups of extremely halophilic archaea in the Danakil Depression datasets[20,21]. For this, we included 61 Danakil MAGs in a preliminary phylogenetic tree containing 488 representatives of archaeal diversity and constructed a phylogenetic tree using 49 concatenated ribosomal proteins with IQ-TREE (v.2.0.3)[59] (Supplementary Fig. 40). The tree was built using the LG + C20 + F + Γ4 model of sequence evolution and support at branches was estimated from 1,000 ultrafast bootstrap replicates. From this analysis, we selected 14 high-quality MAGs (>50% completeness, ≤5% redundancy) representing potential divergent groups of extremely halophilic archaea based on their position compared to other known halophilic archaea. These 14 MAGs were taxonomically classified using GTDB-Tk[27] (v.2.3.0, r207; 1 April 2022) and assigned to families within three GTDB orders: 4 MAGs were assigned to a previously undescribed family belonging to the order 'JAHENH01', which we have named Afararchaeaceae; 9 MAGs were assigned to another previously undescribed family belonging to the order Nanosalinales, which we have named Asbonarchaeaceae; and 1 MAG belonged to a third family in the order Halobacteriales, which we have named Chewarchaeaceae (see taxonomic description above for more details). The pairwise ANI values for the 4 Afararchaeaceae MAGs (Supplementary Fig. 1a) and 9 Asbonarchaeaceae MAGs (Supplementary Fig. 1c) were calculated using FastANI (v.1.34)[60]. The pairwise average amino acid identity (AAI) values for the 4 Afararchaeaceae MAGs (Supplementary Fig. 1c) and 9 Asbonarchaeaceae MAGs (Supplementary Fig. 1d) were calculated using an online calculator[61]. This AAI calculator estimates the AAI using the reciprocal best hits (two-way AAI) between two genomic datasets of proteins.

Metagenome-assembled genome annotation

Coding DNA sequences were predicted with Prodigal (v.2.6.3)[62] and subjected to Pfam[33] and COG[63] functional annotations inside the Anvi'o v.5 pipeline[64]. Genes were also annotated with KofamKOALA[65] and eggNOG-mapper (v.2.1.5)[34]. Additional manual curation was done for the two most complete Afararchaeaceae and Asbonarchaeaceae MAGs (DAL-WCL_na_97C3R and DAL-WCL_45_84C1R, respectively). Further information on gene annotations and functional predictions can be found in Supplementary Data 3 and 4.

Detection of undescribed protein families

We computed family clusters of the proteins predicted for the MAGs of the archaeal families Afararchaeaceae and Asbonarchaeaceae using Mmseqs2 (v.3.0)[66] with relaxed thresholds: minimum percentage of amino acids identity of 30%, *e*-value < 1×10^{-3} and a minimum sequence coverage of 50% (--min-seq-id 0.3 -c 0.5 --cov-mode 2 --cluster-mode 0). To detect families with no homologues in reference databases, we mapped (1) the protein sequences encoded in the MAGs against EggNOG using eggNOG-mapper (v.2)[34] (hits with an *e*-value < 1×10^{-3} were considered as significant); (2) the protein sequences encoded in the MAGs against PfamA domains using HMMER (v.3.3.2)[67] (hits with an *e*-value < 1×10^{-5} were considered as significant); (3) the protein sequences encoded in the MAGs against PfamB domains using HMMER (v.3.3.2)[67] (hits with an *e*-value < 1×10^{-5} were considered as significant); and (4) the coding DNA sequences of the MAGs against RefSeq using Diamond BLASTx[68] ('sensitive' flag, hits with an *e*-value < 1×10^{-3} and query coverage >50% were considered as significant). We only considered families as undescribed if they had no detectable homologues in these databases. To address the taxonomic breadth of these families, we used Diamond BLASTp (v.2.1.7)[68] ('sensitive' flag, hits with an *e*-value < 1×10^{-3} and query coverage >50% were considered as significant) to map the longest sequence of each family against the proteins encoded in a collection of 169,484 genomes spanning the prokaryotic tree of life and including non-cultured species coming from diverse sequencing efforts: the Genomic Catalog of Earth's Microbiomes (GEM)[69], the Global Microbial Gene Catalog (GMGC)[70], the Unified Human Gastrointestinal Genome collection (UHGG)[71] and the Ocean Microbiomics Database (OMD)[72]. We then expanded each protein family with the hits from these databases. If, after expanding, a family incorporated genes with homologues in EggNOG, that family was then discarded from the undescribed family set. We predicted signal peptides and transmembrane domains on the gene families using SignalP (v.6.0)[73] and TMHMM (v.2.0)[74]. Protein families were considered as transmembrane or exported if >80% of their members had a predicted transmembrane domain or a signal peptide, respectively.

Phylogenomic analyses

We collected the proteomes of 192 taxa spanning all major archaeal supergroups (including the Afararchaeaceae and Asbonarchaeaceae). We reconstructed two phylogenomic datasets consisting of 48 ribosomal proteins (RP) and 136 non-ribosomal markers (NM) widely distributed in archaea (Supplementary Fig. 41). The 136 NM dataset was based on curating a set of 200 markers previously shown to be highly conserved across the archaeal domain[18]. To ensure standardized protein-coding gene predictions, all 192 genomes were first run through Prodigal[62]. Next, sequences similar to the RP and NM proteins were identified using BLAST (v.2.10.0)[75] with relatively relaxed criteria (>20% sequence identity over 30% query length) to retrieve even divergent homologues, such as those found in fast-evolving lineages like the DPANN archaea. For each of the 192 taxa, up to 5 of the best BLAST hit sequences were kept and included in a single file for phylogenetic reconstruction. Preliminary trees inferred with FastTree2 (v.2.1.11)[76] under the LG + Γ model were manually examined to identify the correct orthologue for each taxon and to detect cases of contamination, HGT, or paralogy. These spurious sequences were removed and the remaining ones used for reconstruction of a phylogenetic tree. Multiple rounds of manual curation were done in this way until all problematic sequences were removed. Once curated, each orthologous group was aligned with MAFFT L-INS-i (v.7.450)[77] and trimmed with BMGE (v.1.12)[78] (-m BLOSUM30 -b 3 -g 0.2 -h 0.5). We performed a final round of verification of the single-gene trees reconstructed using the more sophisticated LG + C60 + F + Γ4 model in IQ-TREE (v.2.0.3)[59] before concatenating the individually trimmed alignments into two supermatrices (RP and NM). The 192-RP and 192-NM alignments were then subsampled to generate two additional alignments consisting of 87 taxa containing only Euryarchaeota (87-RP and 87-NM) and 104 taxa, including the 87 Euryarchaeota plus 8 Nanosalinaceae and 9 Asbonarchaeaceae (104-RP and 104-NM). These six alignments were then used for ML phylogenetic reconstruction under the LG + C60 + F + Γ4

sequence evolution model (with 1,000 ultrafast bootstrap replicates) using IQ-TREE (v.2.0.3)[59]. For four of the six alignments (87-RP, 104-RP, 87-NM and 104-NM), Bayesian phylogenetic reconstructions were also run using the CAT + GTR model as implemented in PhyloBayes (v.1.8)[79]. Four MCMC chains were run in parallel for each alignment. Although convergence was not reached after 8 months of calculation, a sufficient effective sample size was reached (effsize > 300) while using a burn-in of 3,000 cycles and sampling every 50 generations after the burn-in.

Amino acid composition analysis

We used an in-house Python v.3.10.5 script (https://github.com/bbaker567/phylogenetics) to estimate the frequency of each amino acid in our selection of 192 archaeal taxa for the whole predicted proteomes, as well as for the RP and NM datasets. These frequencies were analysed using principal component analysis (PCA) with ggplot2 (v.3.4.2)[80].

In addition, for each amino acid, the compositional bias between halophiles and non-halophiles was measured for the RP and NM datasets with the *Z*-score from a binomial test of two proportions:

$$Z = \frac{p1 - p2}{\sqrt{p0(1-p0)\left(\frac{1}{n1} + \frac{1}{n2}\right)}}$$

$$p1 = \frac{X1}{n1}, p2 = \frac{X2}{n2}, p0 = \frac{X1 + X2}{n1 + n2}$$

where $X1$ and $X2$ are the total numbers of that amino acid, and $n1$ and $n2$ are the total numbers of all 20 amino acids across halophiles and non-halophiles, respectively. Calculating *Z*-scores in this way assumes that the proportions of an amino acid across halophiles and non-halophiles are approximately normal, with the null hypothesis that $p1 = p2$. $|Z| > 1.96$ indicates rejection of the null hypothesis at a significance level of $P < 0.05$. Amino acids with $|Z| > 1.96$ were considered significantly enriched in halophiles relative to non-halophiles, whereas amino acids with $|Z| < -1.96$ were considered significantly depleted in halophiles relative to non-halophiles. Amino acids were divided into 'Over-represented' ($|Z| > 1.96$), 'Under-represented' ($|Z| < -1.96$) and 'Not significant' ($|Z|$ not statistically significant).

We also implemented the GFmix-DE/IK model by transforming the *b* parameter of the GFmix model[43] (originally designed to represent the ratio of GARP/FYMINK amino acids across all descendant taxa at each branch in a tree) to accommodate amino acid groupings other than GARP/FYMINK, in our case those identified to be biased in extreme halophiles. We then calculated the likelihood of different tree topologies under these variants of the GFmix model with LG + C60 + F + Γ4 (ref. 43). Branch length and alpha shape parameters for each tree tested were estimated using IQ-TREE (v.2.0.3)[59] and then fed into GFmix, specifying the custom enriched and depleted amino acid bins for halophiles versus non-halophiles. We used this approach to calculate the likelihood of four different tree topologies: (1) Nanosalinaceae+Asbonarchaeaceae within DPANN and Methanonatronarchaeia sister to the AHH clade; (2) Nanosalinaceae+Asbonarchaeaceae within DPANN and Methanonatronarchaeia deep within Euryarchaeota; (3) monophyly of the AHH clade, Methanonatronarchaeia and Nanosalinaceae+Asbonarchaeaceae, with Methanonatronarchaeia as the deepest branch and (4) monophyly of the AHH clade, Methanonatronarchaeia and Nanosalinaceae+Asbon archaeaceae, with Nanosalinaceae+Asbonarchaeaceae as the deepest branch (Supplementary Fig. 13).

Progressive removal of compositionally biased sites

To remove the most compositionally biased sites from the sequence alignments, we split them in two on the basis of whether the taxa were classified as extreme halophiles or non-halophiles. We then calculated the ratio of D + E divided by I + K for each alignment site for both the halophiles and non-halophiles sub-alignments. We then divided the D + E/I + K ratio for each halophile sub-alignment site by the corresponding ratio in the non-halophile sub-alignment. When the denominator of one of the ratios was equal to zero, we substituted '0' for '0.1' to still consider the alignment position. Alignment sites were then ranked from the highest to the lowest ratio, using the highest ratio as a proxy for the most biased alignment site. Next, we progressively removed alignment sites in increments of 10% and up to 90%. We also generated alignments by removing only 1% and 5% of the most biased sites. This resulted in 11 alignments for both the RP and NM datasets. These 11 alignments were then used for ML phylogenetic reconstruction under the LG + C60 + F + Γ4 model (with 1,000 ultrafast bootstraps).

In the case of ribosomal proteins, we mapped the acidic amino acid positions on the large ribosomal subunit structures of the extremely halophilic haloarchaeon *Haloarcula marismortui* (PDB[81] accession number 1S72 (ref. 82)) and the non-halophilic methanogen *Methanothermobacter thermautotrophicus* (PDB[81] accession number 4ADX ref. 83). We located these positions on their respective structures using ChimeraX (v.1.7)[84], which was also used to produce a video showing them (Supplementary Video 1).

Orthologous groups and single-gene trees

Orthologous groups (OGs) were identified for all the proteins of the species included in the 192 taxa dataset using OrthoFinder (v.2.5.1)[85] with Diamond BLAST v.2.1.7 (--ultra-sensitive, --query-cover 50% and --id 30%) and an inflation parameter of 1.1. This resulted in 17,827 OGs, which were aligned using MAFFT v.7.450 --auto[77] with default settings and trimmed using trimAl (v.1.2)[86] (-automated1 -resoverlap 0.75 -seqoverlap 75). To avoid poorly resolved single-gene trees due to little phylogenetic information, we removed OGs that presented a trimmed alignment length of less than 60 amino acids. This resulted in 17,288 OGs, which were used to reconstruct individual trees with IQ-TREE (v.2.0.3)[59]. For computational time reasons, the trees of the 200 OGs containing the largest number of sequences were inferred under the LG + C20 + F + Γ4 model of sequence evolution, while the remaining phylogenies were run under LG + C60 + F + Γ4. Statistical support at branches was estimated using 1,000 ultrafast bootstrap replicates. Finally, for OGs containing only two or three sequences, 'bootstrap' samples were artificially generated for subsequent analysis in ALE (v.0.4)[87], corresponding to the single possible unrooted tree topology.

Gene tree-aware ancestral gene content reconstruction

The 17,288 single-gene trees were reconciled with the species tree inferred from the 192-NM dataset using the ALEml_undated algorithm of the ALE suite (v.0.4)[87]. ALE infers, for each gene family, duplications, losses, transfers and originations events along a species tree[87]. The raw relative reconciliation frequencies outputted by ALE were summed for all events. These relative frequency values support an evolutionary event occurring at a given node by incorporating the uncertainty of the reconstructed individual gene tree, as represented by the bootstrap replicates. A few gene families were manually selected on the basis of their patterns of presence/absence and/or HGTs in halophilic groups. The presence probability for the various nodes of interest for each of these gene families mentioned in the text can be found in Supplementary Data 9. ALE also predicts the ancestral copy number for each node in the species tree. Phylogenetic trees were visualized using Figtree v.1.4.4 (http://tree.bio.ed.ac.uk/software/figtree), iTOL (v.6.8)[88] and the ETE3 Toolkit (v.3.1.2)[89].

To detect possible genes of bacterial origin in halophilic archaea, we carried out BLAST (v.2.10.0)[75] searches of the proteins considered by ALE as 'originations' in these archaea against the RefSeq[32] database. Proteins with similar sequences in bacteria were aligned using MAFFT v.7.450 --auto[77] with default settings and trimmed using trimAl (v.1.2)[86] (-automated1). Maximum likelihood trees were then reconstructed with IQ-TREE (v.2.0.3)[59] under the LG + C60 + F + Γ4 model of sequence

evolution. Statistical support at branches was estimated using 1,000 ultrafast bootstrap replicates. Phylogenetic trees were visualized using Figtree v.1.4.4 (http://tree.bio.ed.ac.uk/software/figtree).

Reporting summary

Further information on research design is available in the Nature Portfolio Reporting Summary linked to this article.

Data availability

The MAGs reported in this study have been deposited in GenBank under BioProject number PRJNA901412. All raw data underlying phylogenomic analyses (raw and processed alignments and corresponding phylogenetic trees) and all predicted proteomes have been deposited in Figshare (https://figshare.com/s/353259800b42a4e190eb). Additional data were obtained from public databases, including GTDB (https://gtdb.ecogenomic.org/), Pfam (http://pfam.xfam.org/), COG (https://www.ncbi.nlm.nih.gov/research/cog), RefSeq (https://www.ncbi.nlm.nih.gov/refseq/), eggNOG (http://eggnog5.embl.de/#/app/home), the Genomic Catalog of Earth's Microbiomes (https://genome.jgi.doe.gov/portal/GEMs/GEMs.home.html), the Global Microbial Gene Catalog (https://gmgc.embl.de/), the Unified Human Gastrointestinal Genome collection (http://ftp.ebi.ac.uk/pub/databases/metagenomics/mgnify_genomes/), the Ocean Microbiomics Database (https://microbiomics.io/ocean/) and PDB (https://www.rcsb.org/).

Code availability

Custom code used for data analysis is available on GitHub at https://github.com/bbaker567/phylogenetics.

References

1. Oren, A. Diversity of halophilic microorganisms: environments, phylogeny, physiology, and applications. *J. Ind. Microbiol. Biotechnol.* **28**, 56–63 (2002).
2. Oren, A. Molecular ecology of extremely halophilic Archaea and Bacteria. *FEMS Microbiol. Ecol.* **39**, 1–7 (2002).
3. Narasingarao, P. et al. De novo metagenomic assembly reveals abundant novel major lineage of Archaea in hypersaline microbial communities. *ISME J.* **6**, 81–93 (2012).
4. Ghai, R. et al. New abundant microbial groups in aquatic hypersaline environments. *Sci. Rep.* **1**, 135 (2011).
5. Zhao, D. et al. Comparative genomic insights into the evolution of Halobacteria-associated '*Candidatus* Nanohaloarchaeota'. *mSystems* **7**, e0066922 (2022).
6. Rinke, C. et al. Insights into the phylogeny and coding potential of microbial dark matter. *Nature* **499**, 431–437 (2013).
7. Sorokin, D. Y. et al. Discovery of extremely halophilic, methyl-reducing euryarchaea provides insights into the evolutionary origin of methanogenesis. *Nat. Microbiol.* **2**, 17081 (2017).
8. Aouad, M., Borrel, G., Brochier-Armanet, C. & Gribaldo, S. Evolutionary placement of Methanonatronarchaeia. *Nat. Microbiol.* **4**, 558–559 (2019).
9. Feng, Y. et al. The evolutionary origins of extreme halophilic archaeal lineages. *Genome Biol. Evol.* **13**, evab166 (2021).
10. Martijn, J. et al. Hikarchaeia demonstrate an intermediate stage in the methanogen-to-halophile transition. *Nat. Commun.* **11**, 5490 (2020).
11. Sorokin, D. Y. et al. Reply to 'Evolutionary placement of Methanonatronarchaeia'. *Nat. Microbiol.* **4**, 560–561 (2019).
12. Zhou, H. et al. Metagenomic insights into the environmental adaptation and metabolism of *Candidatus* Haloplasmatales, one archaeal order thriving in saline lakes. *Environ. Microbiol.* **24**, 2239–2258 (2022).
13. Oren, A. Microbial life at high salt concentrations: phylogenetic and metabolic diversity. *Saline Syst.* **4**, 2 (2008).
14. Fukuchi, S., Yoshimune, K., Wakayama, M., Moriguchi, M. & Nishikawa, K. Unique amino acid composition of proteins in halophilic bacteria. *J. Mol. Biol.* **327**, 347–357 (2003).
15. Lanyi, J. K. Salt-dependent properties of proteins from extremely halophilic bacteria. *Bacteriol. Rev.* **38**, 272–290 (1974).
16. Madern, D., Ebel, C. & Zaccai, G. Halophilic adaptation of enzymes. *Extremophiles* **4**, 91–98 (2000).
17. Tadeo, X. et al. Structural basis for the amino acid composition of proteins from halophilic archea. *PLoS Biol.* **7**, e1000257 (2009).
18. Petitjean, C., Deschamps, P., López-García, P., Moreira, D. & Brochier-Armanet, C. Extending the conserved phylogenetic core of Archaea disentangles the evolution of the third domain of life. *Mol. Biol. Evol.* **32**, 1242–1254 (2015).
19. Dombrowski, N., Lee, J.-H., Williams, T. A., Offre, P. & Spang, A. Genomic diversity, lifestyles and evolutionary origins of DPANN archaea. *FEMS Microbiol. Lett.* **366**, fnz008 (2019).
20. Belilla, J. et al. Archaeal overdominance close to life-limiting conditions in geothermally influenced hypersaline lakes at the Danakil Depression, Ethiopia. *Environ. Microbiol.* **23**, 7168–7182 (2021).
21. Belilla, J. et al. Hyperdiverse archaea near life limits at the polyextreme geothermal Dallol area. *Nat. Ecol. Evol.* **3**, 1552–1561 (2019).
22. Kanehisa, M., Sato, Y., Kawashima, M., Furumichi, M. & Tanabe, M. KEGG as a reference resource for gene and protein annotation. *Nucleic Acids Res.* **44**, D457–D462 (2016).
23. Falb, M. et al. Metabolism of halophilic archaea. *Extremophiles* **12**, 177–196 (2008).
24. Albers, S.-V. & Jarrell, K. F. The archaellum: how Archaea swim. *Front. Microbiol.* **6**, 23 (2015).
25. Sasaki, J. & Spudich, J. L. Signal transfer in haloarchaeal sensory rhodopsin – transducer complexes. *Photochem. Photobiol.* **84**, 863–868 (2008).
26. Dassarma, S. et al. Genomic perspective on the photobiology of *Halobacterium* species NRC-1, a phototrophic, phototactic, and UV-tolerant haloarchaeon. *Photosynth. Res.* **70**, 3–17 (2001).
27. Chaumeil, P.-A., Mussig, A. J., Hugenholtz, P. & Parks, D. H. GTDB-Tk: a toolkit to classify genomes with the Genome Taxonomy Database. *Bioinformatics* **36**, 1925–1927 (2020).
28. Chklovski, A., Parks, D. H., Woodcroft, B. J. & Tyson, G. W. CheckM2: a rapid, scalable and accurate tool for assessing microbial genome quality using machine learning. *Nat. Methods* **20**, 1203–1212 (2023).
29. Castelle, C. J. et al. Biosynthetic capacity, metabolic variety and unusual biology in the CPR and DPANN radiations. *Nat. Rev. Microbiol.* **16**, 629–645 (2018).
30. Hamm, J. N. et al. Unexpected host dependency of Antarctic Nanohaloarchaeota. *Proc. Natl Acad. Sci. USA* **116**, 14661–14670 (2019).
31. La Cono, V. et al. Symbiosis between nanohaloarchaeon and haloarchaeon is based on utilization of different polysaccharides. *Proc. Natl Acad. Sci. USA* **117**, 20223–20234 (2020).
32. Pruitt, K. D., Tatusova, T. & Maglott, D. R. NCBI reference sequences (RefSeq): a curated non-redundant sequence database of genomes, transcripts and proteins. *Nucleic Acids Res.* **35**, D61–D65 (2007).
33. Mistry, J. et al. Pfam: the protein families database in 2021. *Nucleic Acids Res.* **49**, D412–D419 (2021).
34. Cantalapiedra, C. P., Hernández-Plaza, A., Letunic, I., Bork, P. & Huerta-Cepas, J. eggNOG-mapper v2: functional annotation, orthology assignments, and domain prediction at the metagenomic scale. *Mol. Biol. Evol.* **38**, 5825–5829 (2021).
35. Rodríguez del Río, Á. et al. Functional and evolutionary significance of unknown genes from uncultivated taxa. *Nature* **626**, 377–384 (2024).

36. Cabello-Yeves, P. J. & Rodriguez-Valera, F. Marine–freshwater prokaryotic transitions require extensive changes in the predicted proteome. *Microbiome* **7**, 117 (2019).
37. Rasmussen, T. How do mechanosensitive channels sense membrane tension? *Biochem. Soc. Trans.* **44**, 1019–1025 (2016).
38. Petitjean, C., Deschamps, P., López-García, P. & Moreira, D. Rooting the Domain Archaea by phylogenomic analysis supports the foundation of the new Kingdom Proteoarchaeota. *Genome Biol. Evol.* **7**, 191–204 (2015).
39. Eme, L. et al. Inference and reconstruction of the heimdallarchaeial ancestry of eukaryotes. *Nature* **618**, 992–999 (2023).
40. Bergsten, J. A review of long-branch attraction. *Cladistics* **21**, 163–193 (2005).
41. Susko, E. & Roger, A. J. Long branch attraction biases in phylogenetics. *Syst. Biol.* **70**, 838–843 (2021).
42. Shimodaira, H. An approximately unbiased test of phylogenetic tree selection. *Syst. Biol.* **51**, 492–508 (2002).
43. Muñoz-Gómez, S. A. et al. Site-and-branch-heterogeneous analyses of an expanded dataset favour mitochondria as sister to known Alphaproteobacteria. *Nat. Ecol. Evol.* **6**, 253–262 (2022).
44. Aouad, M. et al. Extreme halophilic archaea derive from two distinct methanogen Class II lineages. *Mol. Phylogenet. Evol.* **127**, 46–54 (2018).
45. Mahendrarajah, T. A. et al. ATP synthase evolution on a cross-braced dated tree of life. *Nat. Commun.* **14**, 7456 (2023).
46. Kellner, S. et al. Genome size evolution in the Archaea. *Emerg. Top. Life Sci.* **2**, 595–605 (2018).
47. Brehmer, D., Gässler, C., Rist, W., Mayer, M. P. & Bukau, B. Influence of GrpE on DnaK–substrate interactions. *J. Biol. Chem.* **279**, 27957–27964 (2004).
48. Williams, T. A. et al. Integrative modeling of gene and genome evolution roots the archaeal tree of life. *Proc. Natl Acad. Sci. USA* **114**, E4602–E4611 (2017).
49. Giovannoni, S. J. et al. Genome streamlining in a cosmopolitan oceanic bacterium. *Science* **309**, 1242–1245 (2005).
50. Swan, B. K. et al. Prevalent genome streamlining and latitudinal divergence of planktonic bacteria in the surface ocean. *Proc. Natl Acad. Sci. USA* **110**, 11463–11468 (2013).
51. Martin-Cuadrado, A.-B., Ghai, R., Gonzaga, A. & Rodriguez-Valera, F. CO Dehydrogenase genes found in metagenomic fosmid clones from the deep Mediterranean Sea. *Appl. Environ. Microbiol.* **75**, 7436–7444 (2009).
52. Becker, E. A. et al. Phylogenetically driven sequencing of extremely halophilic archaea reveals strategies for static and dynamic osmo-response. *PLoS Genet.* **10**, e1004784 (2014).
53. Groussin, M. et al. Gene acquisitions from Bacteria at the origins of major archaeal clades are vastly overestimated. *Mol. Biol. Evol.* **33**, 305–310 (2016).
54. Nelson-Sathi, S. et al. Acquisition of 1,000 eubacterial genes physiologically transformed a methanogen at the origin of Haloarchaea. *Proc. Natl Acad. Sci. USA* **109**, 20537–20542 (2012).
55. Nelson-Sathi, S. et al. Origins of major archaeal clades correspond to gene acquisitions from bacteria. *Nature* **517**, 77–80 (2015).
56. Gadda, G. & McAllister-Wilkins, E. E. Cloning, expression, and purification of choline dehydrogenase from the moderate halophile *Halomonas elongata*. *Appl. Environ. Microbiol.* **69**, 2126–2132 (2003).
57. Deschamps, P., Zivanovic, Y., Moreira, D., Rodriguez-Valera, F. & López-García, P. Pangenome evidence for extensive interdomain horizontal transfer affecting lineage core and shell genes in uncultured planktonic Thaumarchaeota and Euryarchaeota. *Genome Biol. Evol.* **6**, 1549–1563 (2014).
58. Hedlund, B. P. et al. SeqCode: a nomenclatural code for prokaryotes described from sequence data. *Nat. Microbiol.* **7**, 1702–1708 (2022).
59. Minh, B. Q. et al. IQ-TREE 2: new models and efficient methods for phylogenetic inference in the genomic era. *Mol. Biol. Evol.* **37**, 1530–1534 (2020).
60. Jain, C., Rodriguez-R, L. M., Phillippy, A. M., Konstantinidis, K. T. & Aluru, S. High throughput ANI analysis of 90K prokaryotic genomes reveals clear species boundaries. *Nat. Commun.* **9**, 5114 (2018).
61. Rodriguez-R, L. M. & Konstantinidis, K. T. Bypassing cultivation to identify bacterial species: culture-independent genomic approaches identify credibly distinct clusters, avoid cultivation bias, and provide true insights into microbial species. *Microbe Mag.* **9**, 111–118 (2014).
62. Hyatt, D. et al. Prodigal: prokaryotic gene recognition and translation initiation site identification. *BMC Bioinformatics* **11**, 119 (2010).
63. Tatusov, R. L., Galperin, M. Y., Natale, D. A. & Koonin, E. V. The COG database: a tool for genome-scale analysis of protein functions and evolution. *Nucleic Acids Res.* **28**, 33–36 (2000).
64. Eren, A. M. et al. Anvi'o: an advanced analysis and visualization platform for 'omics data. *PeerJ* **3**, e1319 (2015).
65. Aramaki, T. et al. KofamKOALA: KEGG Ortholog assignment based on profile HMM and adaptive score threshold. *Bioinformatics* **36**, 2251–2252 (2020).
66. Steinegger, M. & Söding, J. MMseqs2 enables sensitive protein sequence searching for the analysis of massive data sets. *Nat. Biotechnol.* **35**, 1026–1028 (2017).
67. Eddy, S. R. Accelerated profile HMM searches. *PLoS Comput. Biol.* **7**, e1002195 (2011).
68. Buchfink, B., Xie, C. & Huson, D. H. Fast and sensitive protein alignment using DIAMOND. *Nat. Methods* **12**, 59–60 (2015).
69. Nayfach, S. et al. A genomic catalog of Earth's microbiomes. *Nat. Biotechnol.* **39**, 499–509 (2021).
70. Coelho, L. P. et al. Towards the biogeography of prokaryotic genes. *Nature* **601**, 252–256 (2022).
71. Almeida, A. et al. A unified catalog of 204,938 reference genomes from the human gut microbiome. *Nat. Biotechnol.* **39**, 105–114 (2021).
72. Paoli, L. et al. Biosynthetic potential of the global ocean microbiome. *Nature* **607**, 111–118 (2022).
73. Almagro Armenteros, J. J. et al. SignalP 5.0 improves signal peptide predictions using deep neural networks. *Nat. Biotechnol.* **37**, 420–423 (2019).
74. Krogh, A., Larsson, B., von Heijne, G. & Sonnhammer, E. L. L. Predicting transmembrane protein topology with a hidden Markov model: application to complete genomes. *J. Mol. Biol.* **305**, 567–580 (2001).
75. Altschul, S. F., Gish, W., Miller, W., Myers, E. W. & Lipman, D. J. Basic local alignment search tool. *J. Mol. Biol.* **215**, 403–410 (1990).
76. Price, M. N., Dehal, P. S. & Arkin, A. P. FastTree 2 – approximately maximum-likelihood trees for large alignments. *PLoS ONE* **5**, e9490 (2010).
77. Katoh, K. & Standley, D. M. MAFFT multiple sequence alignment software version 7: improvements in performance and usability. *Mol. Biol. Evol.* **30**, 772–780 (2013).
78. Criscuolo, A. & Gribaldo, S. BMGE (Block Mapping and Gathering with Entropy): a new software for selection of phylogenetic informative regions from multiple sequence alignments. *BMC Evol. Biol.* **10**, 210 (2010).
79. Lartillot, N. PhyloBayes: Bayesian phylogenetics using site-heterogeneous models. in *Phylogenetics in the Genomic Era* (eds Scornavacca, C. et al.) 1.5:1–1.5:16 (HAL Open Science, 2020).
80. Wickham, H. *ggplot2: Elegant Graphics for Data Analysis* (Springer, 2009).

81. Berman, H. M. et al. The Protein Data Bank. *Nucleic Acids Res.* **28**, 235–242 (2000).
82. Klein, D. J., Moore, P. B. & Steitz, T. A. The roles of ribosomal proteins in the structure assembly, and evolution of the large ribosomal subunit. *J. Mol. Biol.* **340**, 141–177 (2004).
83. Greber, B. J. et al. Cryo-EM structure of the archaeal 50S ribosomal subunit in complex with initiation factor 6 and implications for ribosome evolution. *J. Mol. Biol.* **418**, 145–160 (2012).
84. Pettersen, E. F. et al. UCSF ChimeraX: structure visualization for researchers, educators, and developers. *Protein Sci.* **30**, 70–82 (2021).
85. Emms, D. M. & Kelly, S. OrthoFinder: phylogenetic orthology inference for comparative genomics. *Genome Biol.* **20**, 238 (2019).
86. Capella-Gutiérrez, S., Silla-Martínez, J. M. & Gabaldón, T. trimAl: a tool for automated alignment trimming in large-scale phylogenetic analyses. *Bioinformatics* **25**, 1972–1973 (2009).
87. Szöllősi, G. J., Rosikiewicz, W., Boussau, B., Tannier, E. & Daubin, V. Efficient exploration of the space of reconciled gene trees. *Syst. Biol.* **62**, 901–912 (2013).
88. Letunic, I. & Bork, P. Interactive Tree Of Life (iTOL) v5: an online tool for phylogenetic tree display and annotation. *Nucleic Acids Res.* **49**, W293–W296 (2021).
89. Huerta-Cepas, J., Serra, F. & Bork, P. ETE 3: reconstruction, analysis, and visualization of phylogenomic data. *Mol. Biol. Evol.* **33**, 1635–1638 (2016).

Acknowledgements

D.M. and L.E were supported by grants from the European Research Council (ERC Advanced grant 787904 and ERC Starting grant 803151, respectively). This work was also supported by the Moore-Simons Project Call on the Origin of the Eukaryotic Cell, Simons Foundation 812811 (A.J.R, E.S. and L.E.), Moore Foundation GBMF9739 (P.L.-G.), and ANR DArchFolds ANR-22-CE02-0012-02 (D.M., P.L.-G. and L.E.). A.R.d.R. was supported by 'la Caixa' Foundation (ID 100010434, fellowship code LCF/BQ/DI18/11660009, the European Union's Horizon 2020 research and innovation programme under Marie Skłodowska-Curie grant agreement No. 713673) and by an EMBO Scientific Exchange Grant. We thank P. Deschamps for help in managing our bioinformatic cluster; A. Oren for advice on taxonomic descriptions; and the Iris Foundation for the continuous support of our work on the microbial diversity of the Danakil Depression.

Author contributions

D.M., P.L.-G. and L.E. designed the study. A.G.-P. and B.A.B. annotated the archaeal MAGs. A.R.d.R., B.A.B. and J.H.-C. studied the protein families. C.G.P.M., A.J.R. and E.S. conceived the binomial methods to identify significant shifts in amino acid composition, and E.S. implemented the changes of the GFmix model in the GFmix software. B.A.B., L.E., D.M., C.G.P.M., A.J.R. and E.S. carried out phylogenetic analyses. B.A.B., L.E., P.L.-G. and D.M. wrote the paper with contributions from all authors.

Competing interests

The authors declare no competing interests.

Additional information

Extended data is available for this paper at https://doi.org/10.1038/s41564-024-01647-4.

Supplementary information The online version contains supplementary material available at https://doi.org/10.1038/s41564-024-01647-4.

Correspondence and requests for materials should be addressed to Laura Eme or David Moreira.

Peer review information *Nature Microbiology* thanks Aharon Oren, Tom Williams and the other, anonymous, reviewer(s) for their contribution to the peer review of this work.

https://doi.org/10.1038/s41564-024-01647-4

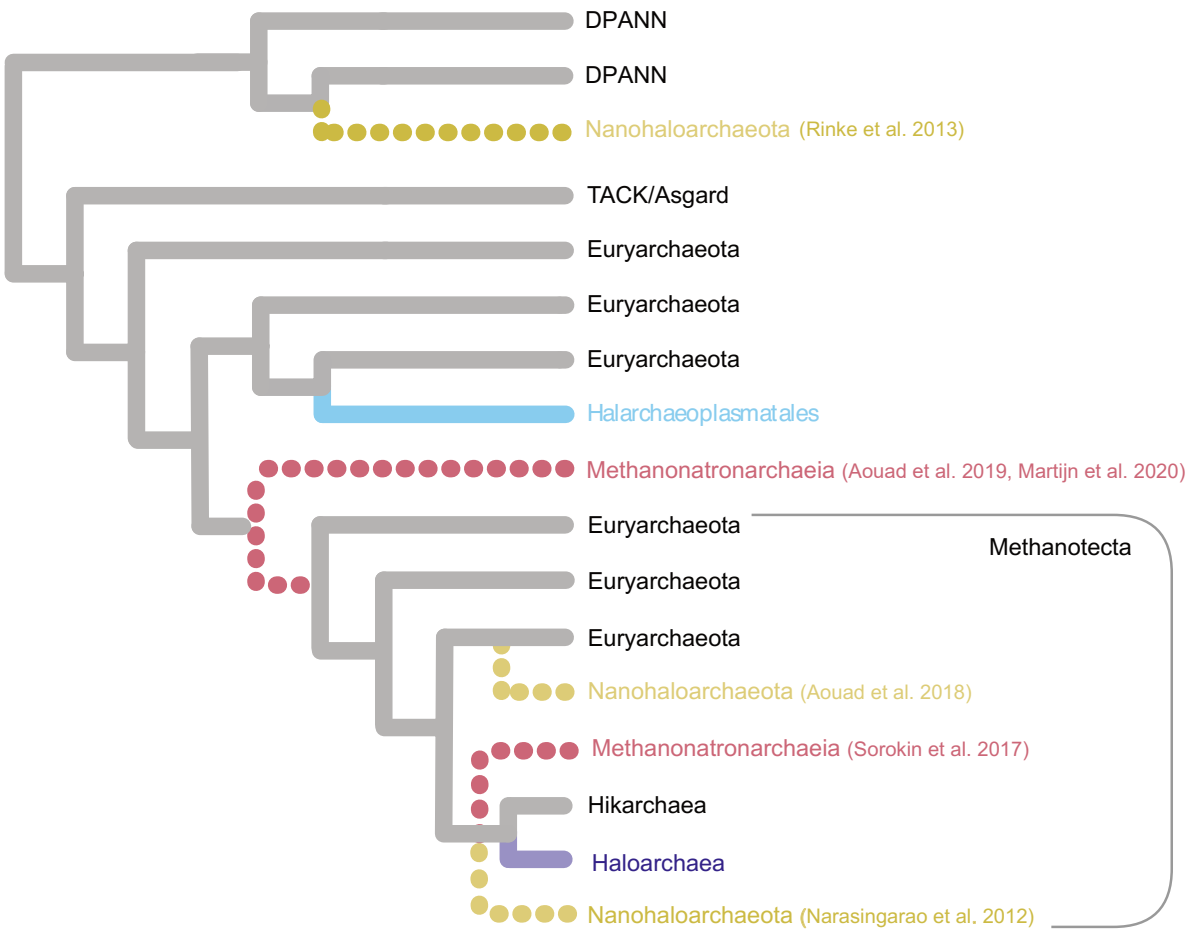

Extended Data Fig. 1 | Schematic tree showing the phylogenetic position of extremely halophilic archaeal groups (colored branches) proposed in previous articles. Branches that have been found at different places in the tree of archaea are indicated with dashed lines (Narasingarao et al. 2012[3], Rinke et al. 2013[6], Sorokin et al. 2017[7], Aouad et al. 2018[44], Aouad et al. 2019[8], Martijn et al. 2020[10]).

https://doi.org/10.1038/s41564-024-01647-4

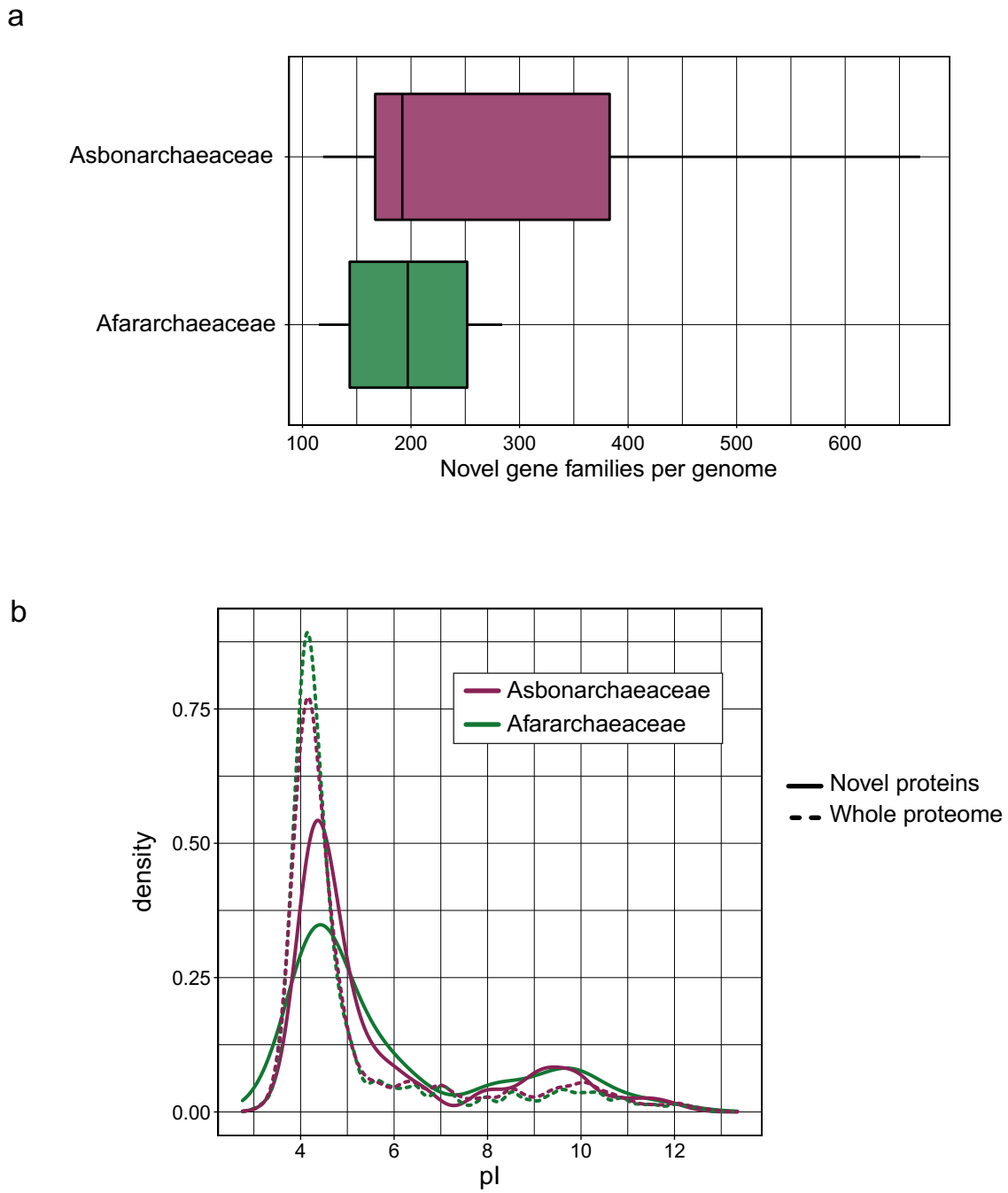

Extended Data Fig. 2 | Number and isoelectric point of novel gene families identified in the Asbonarchaeaceae and Afararchaeaceae MAGs. (a) The average number of novel genes in the nine asbonarchaeal and four afarachaeal MAGs described in this study. Data are represented as boxplots where the middle line is the median, the lower and upper hinges correspond to the first and third quartiles, the upper whisker extends from the hinge to the largest value no further than 1.5 × IQR from the hinge (where IQR is the interquartile range) and the lower whisker extends from the hinge to the smallest value at most 1.5 × IQR of the hinge, while data beyond the end of the whiskers are outlying points that are plotted individually. **(b)** The isoelectric point of these novel proteins (solid lines) compared to the average isoelectric point of the whole proteomes (dashed lines).

https://doi.org/10.1038/s41564-024-01647-4

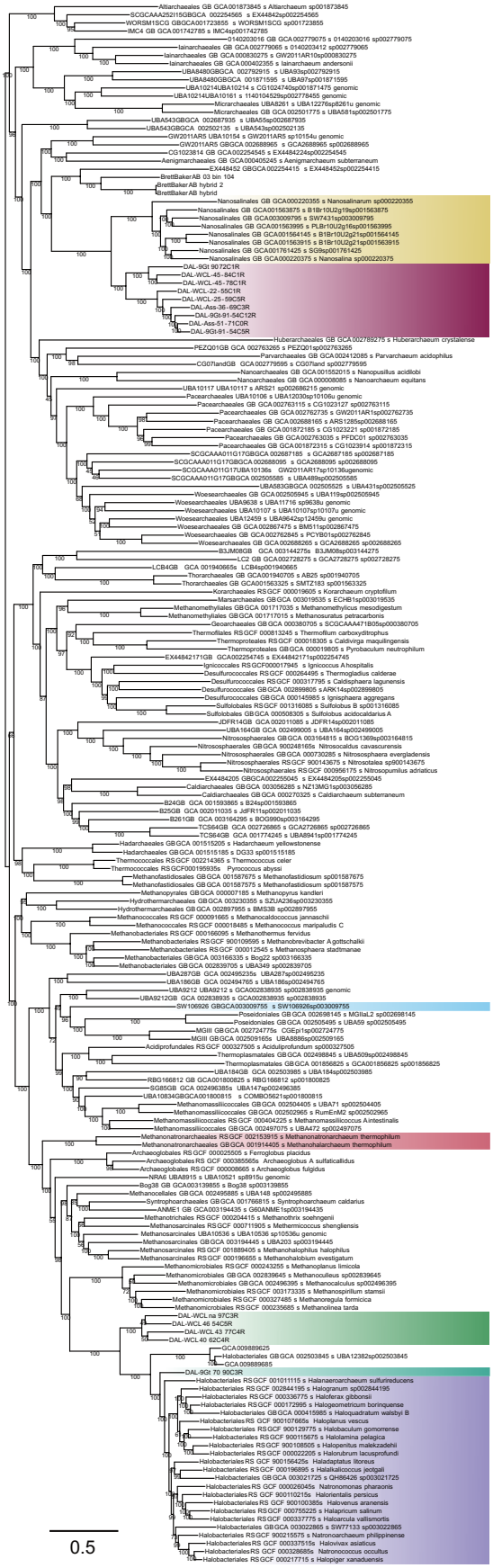

Extended Data Fig. 3 | Maximum likelihood phylogeny of 192 archaea based on the NM dataset. The ML tree was inferred with the LG + C60 + F + Γ4 model of sequence evolution with 1,000 ultrafast bootstraps as implemented via IQ-TREE. The scale bar indicates the expected average number of substitutions per site. Extremely halophilic archaea are indicated in color.

https://doi.org/10.1038/s41564-024-01647-4

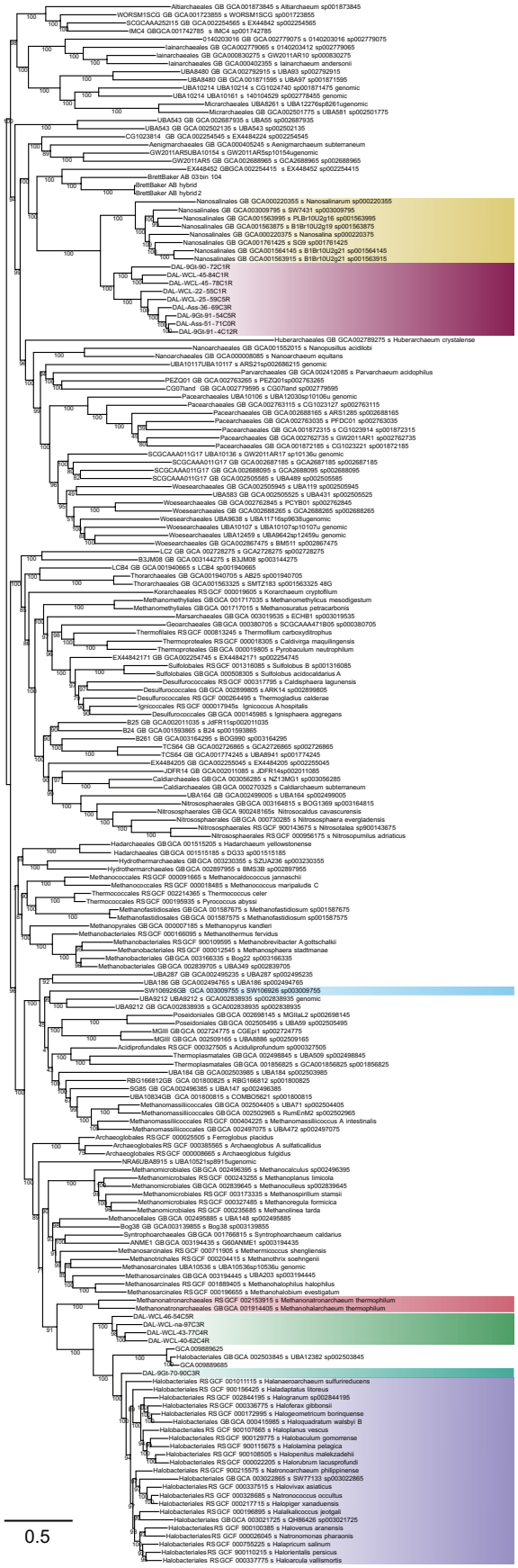

Extended Data Fig. 4 | Maximum likelihood phylogeny of 192 archaea based on the RP dataset. The ML tree was inferred with the LG + C60 + F + Γ4 model of sequence evolution with 1,000 ultrafast bootstraps as implemented via IQ-TREE. The scale bar indicates the expected average number of substitutions per site. Extremely halophilic archaea are indicated in color.

https://doi.org/10.1038/s41564-024-01647-4

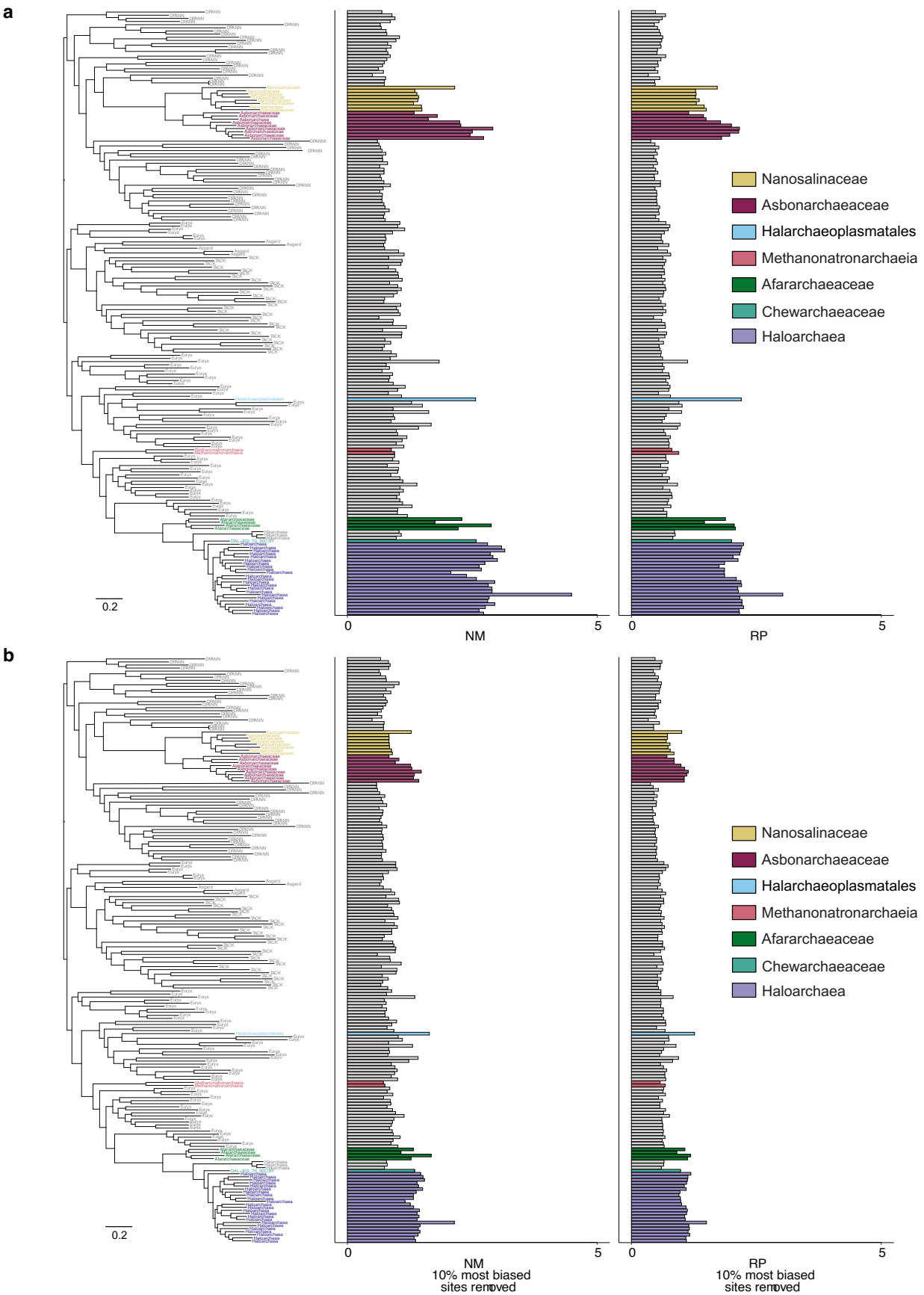

Extended Data Fig. 5 | See next page for caption.

https://doi.org/10.1038/s41564-024-01647-4

Extended Data Fig. 5 | Halophilic-specific amino acid compositional biases along the phylogeny of 192 archaeal taxa. (a) The ratio of [D + E/I + K] amino acids of 192 archaeal taxa was calculated along the untreated NM and RP alignments (39,385 and 6,792 amino acid positions, respectively). **(b)** 10% of the most biased sites (that is, those with the highest ratio) were removed from the NM and RP alignments. Distinct halophilic clades are indicated in color, including the Nanosalinaceae (sand), Asbonarchaeaceae (wine), Halarchaeoplasmatales (cyan), Methanonatronarchaeia (rose), Afarachaeaceae (green), and Haloarchaea (indigo). The scale bar indicates the expected average number of substitutions per site.

https://doi.org/10.1038/s41564-024-01647-4

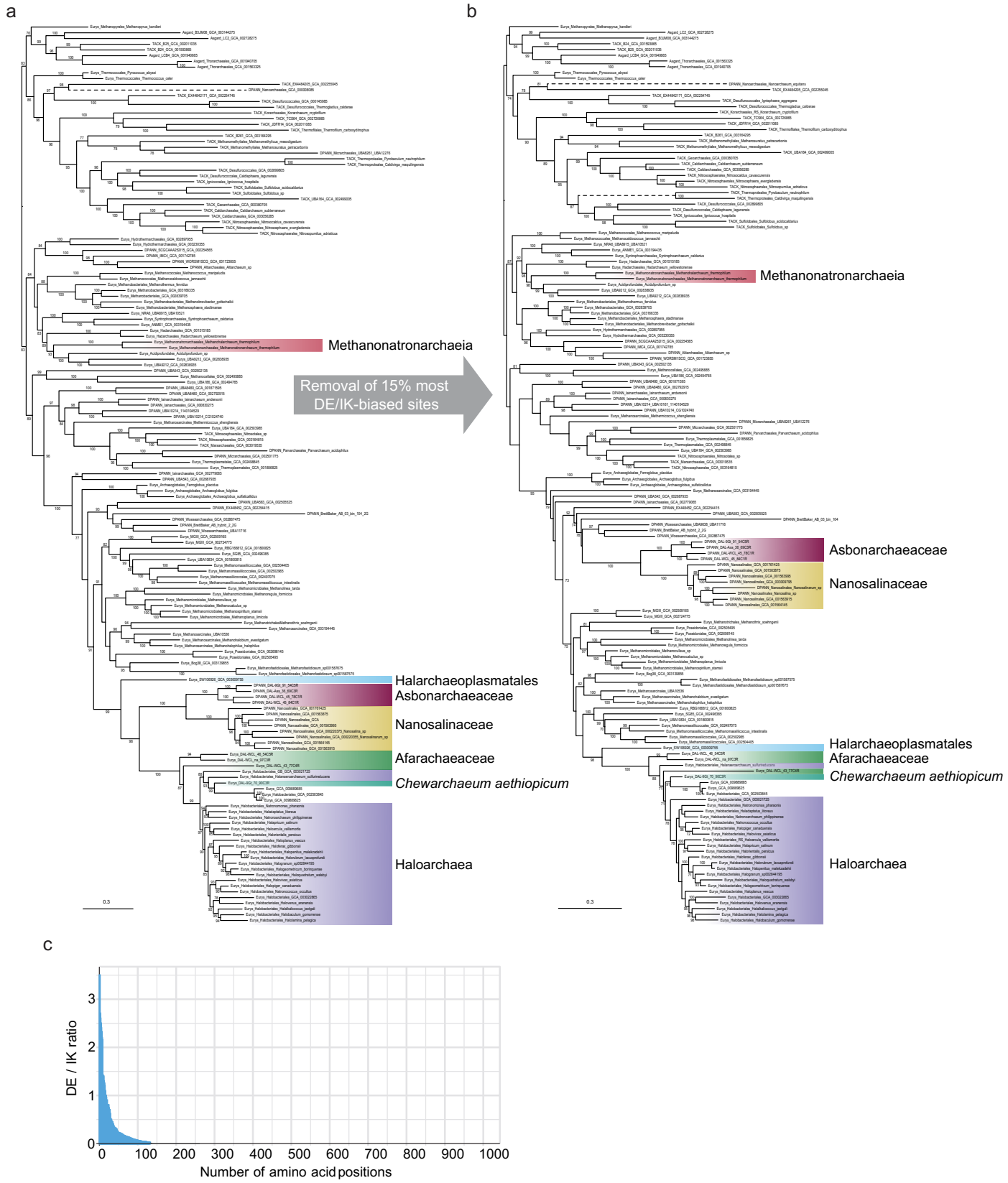

Extended Data Fig. 6 | Impact of compositional bias on the phylogeny of archaeal ATP synthase. Maximum likelihood phylogenetic trees based on the concatenation of ATP synthase subunits A and B **(a)** before and **(b)** after removal of 15% of sites with the highest D + E/I + K ratio. Notice the shift in the position of the Nanosalinaceae+Asbonarchaeaceae group. The trees were reconstructed using the LG + C60 + F + Γ4 model of sequence evolution. Numbers at branches indicate 1,000 ultrafast bootstrap support values. Only values > 70% are indicated. The scale bar indicates the expected average number of substitutions per site. **(c)** D + E/I + K ratio for all sites in the ATP synthase subunits A and B dataset ordered from highest to lowest values.

https://doi.org/10.1038/s41564-024-01647-4

a

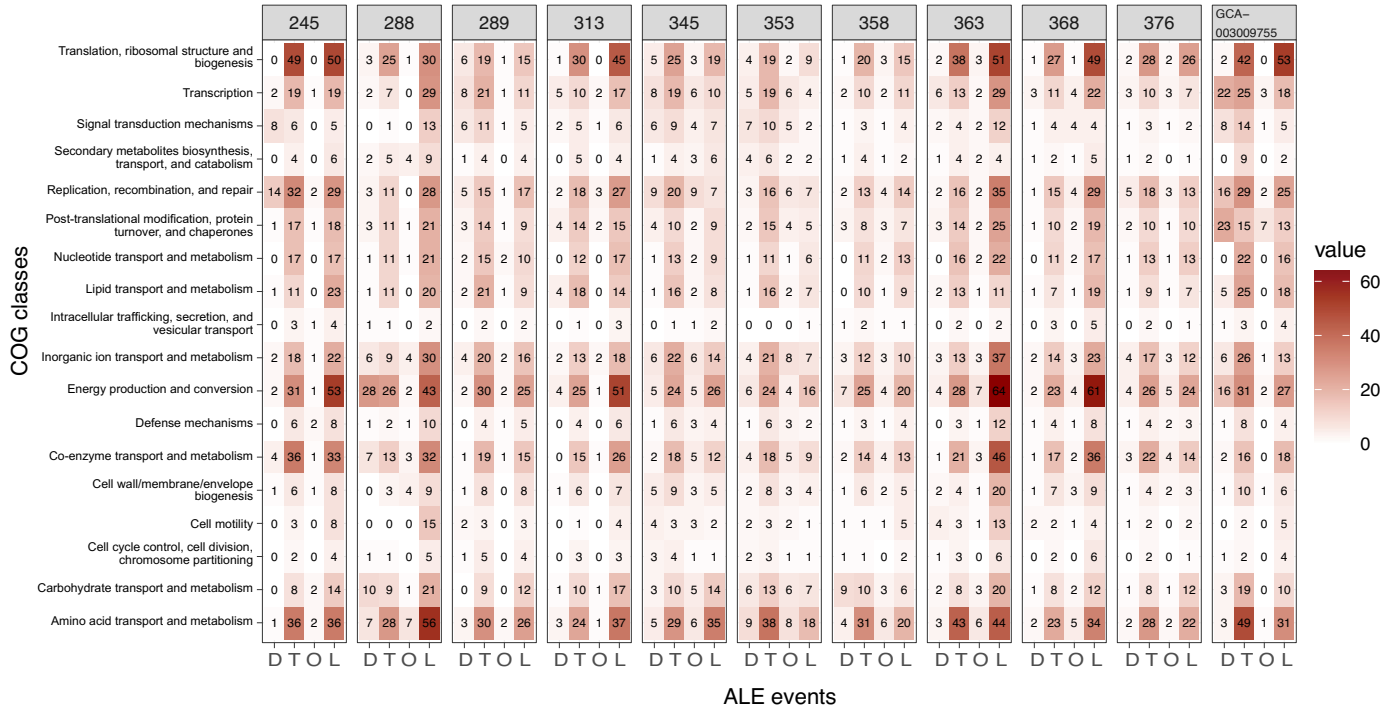

b

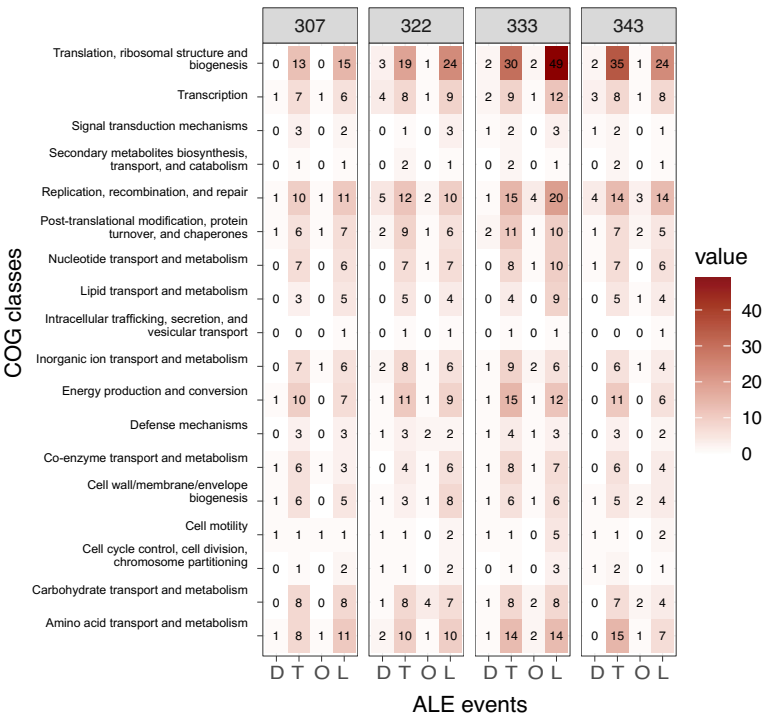

Extended Data Fig. 7 | Heat map of the number of gene duplications, transfers, originations, and losses in various archaeal halophilic lineages according to their COG classification. The counts were obtained using the amalgamated likelihood estimation (ALE) tree reconciliation method on the set of 17,288 orthologous genes present in the 192-taxa genomic dataset for several nodes within the **(a)** Euryarchaeota and the **(b)** DPANN archaea (see Methods). Node numbers correspond to the nodes in the complete tree shown in Supplementary Fig. 18.

https://doi.org/10.1038/s41564-024-01647-4

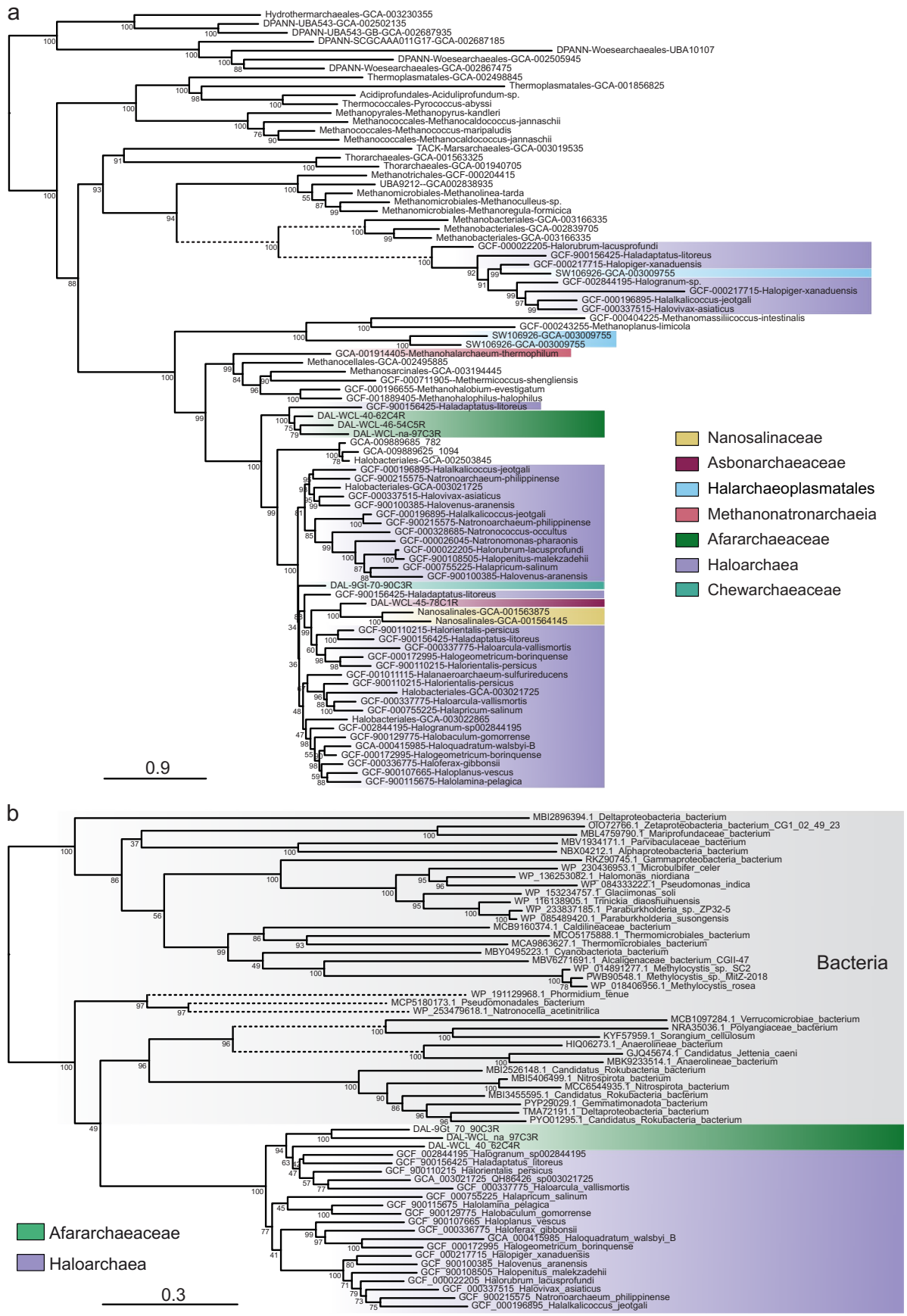

Extended Data Fig. 8 | Maximum likelihood trees showing cases of horizontal gene transfer involving archaeal halophilic lineages. (a) NhaP-type Na + / H+ and K + /H+ antiporters. **(b)** choline dehydrogenase BetA. The trees were constructed with the LG + C60 + F + Γ4 model of sequence evolution. Dashed branches have been shortened to half of their actual length. The scale bar indicates the expected average number of substitutions per site.

nature portfolio

Corresponding author(s): David Moreira
Laura Eme

Last updated by author(s): Jan 11, 2024

Reporting Summary

Nature Portfolio wishes to improve the reproducibility of the work that we publish. This form provides structure for consistency and transparency in reporting. For further information on Nature Portfolio policies, see our Editorial Policies and the Editorial Policy Checklist.

Statistics

For all statistical analyses, confirm that the following items are present in the figure legend, table legend, main text, or Methods section.

n/a	Confirmed	
☐	☒	The exact sample size (*n*) for each experimental group/condition, given as a discrete number and unit of measurement
☐	☒	A statement on whether measurements were taken from distinct samples or whether the same sample was measured repeatedly
☐	☒	The statistical test(s) used AND whether they are one- or two-sided *Only common tests should be described solely by name; describe more complex techniques in the Methods section.*
☐	☒	A description of all covariates tested
☒	☐	A description of any assumptions or corrections, such as tests of normality and adjustment for multiple comparisons
☐	☒	A full description of the statistical parameters including central tendency (e.g. means) or other basic estimates (e.g. regression coefficient) AND variation (e.g. standard deviation) or associated estimates of uncertainty (e.g. confidence intervals)
☐	☒	For null hypothesis testing, the test statistic (e.g. *F*, *t*, *r*) with confidence intervals, effect sizes, degrees of freedom and *P* value noted *Give P values as exact values whenever suitable.*
☒	☐	For Bayesian analysis, information on the choice of priors and Markov chain Monte Carlo settings
☒	☐	For hierarchical and complex designs, identification of the appropriate level for tests and full reporting of outcomes
☒	☐	Estimates of effect sizes (e.g. Cohen's *d*, Pearson's *r*), indicating how they were calculated

Our web collection on statistics for biologists contains articles on many of the points above.

Software and code

Policy information about availability of computer code

Data collection	Complete predicted proteomes of diverse archaea were downloaded from public databases (GTDB and RefSeq) through their webpages (https://gtdb.ecogenomic.org/downloads and https://www.ncbi.nlm.nih.gov/refseq/, respectively).
Data analysis	Average nucleotide identity (ANI) calculation: FastANI v1.34. Average amino acid identity (AAI) calculation: AAI calculator (http://enve-omics.ce.gatech.edu/aai/) Prediction of Coding DNA Sequences (CDSs): Prodigal v2.6.3. Functional annotation of genes: Anvi'o v5, KofamKOALA (https://www.genome.jp/tools/kofamkoala/), and eggNOG-mapper v2.1.5. Prediction of signal peptides and transmembrane domains: SignalP v6.0 and TMHMM v2.0. Sequence similarity searches: HMMER v3.3.2, Diamond BLAST v2.1.7, and BLAST v2.10.0. Multiple sequence alignment: MAFFT v7.450. Trimming of multiple sequence alignments: BMGE v1.12 and trimAl v1.2. Reconstruction of single protein phylogenetic trees: FastTree2 v2.1.11 and IQ-TREE v2.0.3.

Reconstruction of multi-marker phylogenetic trees: IQ-TREE v2.0.3 and PhyloBayes v1.8.

Visualization of phylogenetic trees: Figtree v.1.4.4 , iTOL v6.8, and the ETE3 Toolkit v.3.1.2.

Clustering of orthologous protein sequences: MMseqs2 v3.0 and OrthoFinder v2.5.1.

Amino acid sequence composition analysis: in-house Python v3.10.5 script (https://github.com/bbaker567/phylogenetics).

Principal component analysis: R v4.3.1 and ggplot2 v3.4.2.

Tree reconciliation analysis: ALE suite v0.4.

Protein structure visualization: ChimeraX v1.7.

For manuscripts utilizing custom algorithms or software that are central to the research but not yet described in published literature, software must be made available to editors and reviewers. We strongly encourage code deposition in a community repository (e.g. GitHub). See the Nature Portfolio guidelines for submitting code & software for further information.

Data

Policy information about availability of data

All manuscripts must include a data availability statement. This statement should provide the following information, where applicable:

- Accession codes, unique identifiers, or web links for publicly available datasets
- A description of any restrictions on data availability
- For clinical datasets or third party data, please ensure that the statement adheres to our policy

The MAGs reported in this study have been deposited in GenBank under BioProject number PRJNA901412. All raw data underlying phylogenomic analyses (raw and processed alignments and corresponding phylogenetic trees) and all predicted proteomes have been deposited into Figshare (https://figshare.com/s/353259800b42a4e190eb). Additional data were obtained from public databases, including GTDB (https://gtdb.ecogenomic.org/), Pfam (http://pfam.xfam.org/), COG (https://www.ncbi.nlm.nih.gov/research/cog), RefSeq (https://www.ncbi.nlm.nih.gov/refseq/), eggNOG (http://eggnog5.embl.de/#/app/home), the Genomic Catalog of Earth's Microbiomes (https://genome.jgi.doe.gov/portal/GEMs/GEMs.home.html), the Global Microbial Gene Catalog (https://gmgc.embl.de/), the Unified Human Gastrointestinal Genome collection (http://ftp.ebi.ac.uk/pub/databases/metagenomics/mgnify_genomes/), the Ocean Microbiomics Database (https://microbiomics.io/ocean/), and PDB (https://www.rcsb.org/).

Research involving human participants, their data, or biological material

Policy information about studies with human participants or human data. See also policy information about sex, gender (identity/presentation), and sexual orientation and race, ethnicity and racism.

Reporting on sex and gender	N/A
Reporting on race, ethnicity, or other socially relevant groupings	N/A
Population characteristics	N/A
Recruitment	N/A
Ethics oversight	N/A

Note that full information on the approval of the study protocol must also be provided in the manuscript.

Field-specific reporting

Please select the one below that is the best fit for your research. If you are not sure, read the appropriate sections before making your selection.

☒ Life sciences ☐ Behavioural & social sciences ☐ Ecological, evolutionary & environmental sciences

For a reference copy of the document with all sections, see nature.com/documents/nr-reporting-summary-flat.pdf

Life sciences study design

All studies must disclose on these points even when the disclosure is negative.

Sample size	We analyzed 192 proteomes from taxa selected to represent all known archaeal diversity while keeping a dataset size compatible with the computationally-intensive maximum likelihood and Bayesian phylogenetic analyses.
Data exclusions	Some of our phylogenetic analyses were based on exclusion of compositionally biased sequence data. We developed an index estimate this bias based on the well-known enrichment in acidic amino acids in halophilic archaea.

Replication	Robustness and reliability of phylogenetic analyses were assessed using 1000 ultrafast bootstrap replicates for all maximum likelihood analyses, as is commonly done in the field.
Randomization	Randomization is not necessary to a study using phylogenetic approaches because these approaches rely on the comparison of evolutionary relationships between species, rather than on random assignment of treatments or control groups. Phylogenetic analyses are not affected by the same sources of bias as experimental designs, such as confounding variables or selection bias. Therefore, while randomization is a useful tool in many types of research, it is not essential in studies using phylogenetics and comparative genomics.
Blinding	Blinding was not relevant to our analyses since there was no group allocation during data collection and analysis.

Reporting for specific materials, systems and methods

We require information from authors about some types of materials, experimental systems and methods used in many studies. Here, indicate whether each material, system or method listed is relevant to your study. If you are not sure if a list item applies to your research, read the appropriate section before selecting a response.

Materials & experimental systems

n/a	Involved in the study
☒	☐ Antibodies
☒	☐ Eukaryotic cell lines
☒	☐ Palaeontology and archaeology
☒	☐ Animals and other organisms
☒	☐ Clinical data
☒	☐ Dual use research of concern
☒	☐ Plants

Methods

n/a	Involved in the study
☒	☐ ChIP-seq
☒	☐ Flow cytometry
☒	☐ MRI-based neuroimaging